High-resolution QTL mapping with Diversity Outbred mice identifies genetic variants that impact gut microbiome composition

Florencia Schlamp[*,1], David Y Zhang[*], Juan Felipe Beltrán[†], Elissa J Cosgrove[*], Petr Simecek[‡,§], Matthew Edwards[*], Julia K Goodrich[*], Ruth E Ley[**], Allan Pack[††], Gary A Churchill[‡], Andrew G Clark[*,1]

Author Affiliations

* Department of Molecular Biology and Genetics, Cornell University, Ithaca NY 14850, USA.

† Department of Biomedical Engineering, Cornell University, Ithaca NY 14850, USA.

‡ The Jackson Laboratory, Bar Harbor ME 04609, USA.

§ Central European Institute of Technology (CEITEC), Masaryk University, Brno 62500, Czech Republic.

** Department of Microbiome Science, Max Planck Institute for Developmental Biology, Tübingen 72026, Germany.

†† Department of Medicine, Perelman School of Medicine at the University of Pennsylvania, Philadelphia PA 19104, USA.

NCBI SRA BioProject ID: PRJNA639769

18 **DO mice host-microbiome associations**

19 **KEYWORDS**: Diversity Outbred mice; Microbiome; QTL mapping

20 [1]Corresponding authors: AGC or FS, Cornell University, Biotechnology Building 227,

21 526 Campus Rd, Ithaca NY 14853. E-mail: ac347@cornell.edu, mfs97@cornell.edu

22 **ABSTRACT**

23 The composition of the gut microbiome is impacted by a complex array of factors, from

24 nutrient composition and availability, to physical factors like temperature, pH, and flow

25 rate, as well as interactions among the members of the microbial community. Many of

26 these factors are affected by the host, raising the question of how host genetic variation

27 impacts microbiome composition. Though human studies confirm this type of role for

28 host genetics, its overall importance is still a subject of debate and remains difficult to

29 study. The mouse model, by allowing the strict control of genetics, nutrition, and other

30 environmental factors, has provided an excellent opportunity to extend this work, and

31 the Diversity Outbred (DO) mice in particular present a chance to pinpoint host genetic

32 variants that influence microbiome composition at different levels of generality. Here, we

33 apply 16S rRNA gene sequencing to fecal samples of 247 DO male mice to estimate

34 heritability and perform taxon-specific QTL mapping of microbial relative abundances

35 revealing an increasingly heterogeneous picture of host function and microbial taxa at

36 the host-microbiome interface. We present the first report of significant heritability of

37 phylum Tenericutes in mice, and find novel QTL-spanning genes involved in

38 antibacterial pathways, immune and inflammatory disease, and lipid metabolism.

INTRODUCTION

The gastrointestinal tract of all vertebrates, including humans, harbors a complex ecological community of highly diverse microbes referred to as the gut microbiota. The microbiota colonizes the gut for the first time during the birth of the host, and its composition is influenced by many factors during the host's life such as disease, diet, and antibiotics (FRANCINO 2016; BATTAGLIOLI AND KASHYAP 2018; DUDEK-WICHER *et al.* 2018; DASH *et al.* 2019). Variation in the human gut microbiome composition has also already been associated with host immune responses (ROUND AND MAZMANIAN 2009; GARRETT *et al.* 2010; VEIGA *et al.* 2010), metabolic phenotypes (TURNBAUGH *et al.* 2009; RIDAURA *et al.* 2013), and diseases such as obesity (LEY *et al.* 2005), heart disease (FAVA *et al.* 2006), and diabetes (WEN *et al.* 2008). Given the roles of the gut microbiome in complex human diseases, it is important to characterize the factors that impact microbiome composition.

While it is clear that the gut microbiome composition is strongly impacted by environmental exposures (ROTHSCHILD *et al.* 2018), the role of host genetics has only recently been implicated (GOODRICH *et al.* 2014; BLEKHMAN *et al.* 2015; GOODRICH *et al.* 2016). Studies have identified multiple genetic variants significantly associated with specific bacterial taxon abundances (DAVENPORT *et al.* 2015; BONDER *et al.* 2016; TURPIN *et al.* 2016; WANG *et al.* 2016; GOODRICH *et al.* 2017; IGARTUA *et al.* 2017; ROTHSCHILD *et al.* 2018) despite the observation that generally the primary determinants of microbiome composition are non-genetic (ROTHSCHILD *et al.* 2018). The relationship between genetic and non-genetic determinants is complex, as in the case of diet, which can influence the variability of complex traits by reshaping the gut microbiome

62 (VOROBYEV *et al.* 2019). Overall, it is clear that host-microbiome relationships are
63 impacted by interactions between genetics and environment to drive both community
64 composition and host traits (KURILSHIKOV *et al.* 2020). Human genetic studies have
65 significant limitations for accurate assessment of genetic effects on the microbiome,
66 including accessibility to large and diverse sample populations as well as a general lack
67 of control over confounding variables like diet, thus only detecting the strongest genetic
68 effects. This lack of experimental control can be circumvented through studies in model
69 organisms, which would allow us to better characterize host-microbiome relationships
70 and increase our chances of identifying genetic effects.

71 The mouse model, with the ability to control diet, provides a better opportunity to
72 dissect genetic and environmental factors impacting microbiome composition and has
73 been successful in this endeavor using inbred strains. Quantitative trait locus (QTL)
74 mapping efforts show that gut microbiota composition is a polygenic trait, with clearly
75 mappable genetic factors influencing the gut microbiome composition (BENSON *et al.*
76 2010; MCKNITE *et al.* 2012; SNIJDERS *et al.* 2016). Standard QTL mapping approaches
77 have low mapping resolution, however, and advanced intercross lines provide one
78 excellent means of improving mapping resolution. BELHEOUANE *et al.* (2017) performed
79 genetic and 16S rRNA gene analysis of skin microbiomes of a collection of 15-
80 generation advanced intercross lines, and demonstrated that the improved mapping
81 resolution also improved the specificity and significance of genetic associations. It is
82 clear that the mouse model will provide further opportunities to dissect the means by
83 which the host genome can modulate microbiome composition. A logical next step is a

84 mapping experiment to identify portions of the genome that influence functional
85 pathways that modulate the microbiome.

86 Here we extend the analysis of the link between the host genome and microbiome
87 using the Diversity Outbred mouse model. The Diversity Outbred (DO) population is a
88 heterogeneous mouse stock derived from the same eight progenitor lines (A/J,
89 C57BL/6J, 129S1/SvImJ, NOD/ShiLtJ, NZO/HlLtJ, CAST/EiJ, PWK/PhJ, and WSB/EiJ)
90 used to establish the Collaborative Cross (CC) (COLLABORATIVE CROSS CONSORTIUM
91 2012). Mice from the CC lines at early stages of inbreeding were used to establish the
92 DO population, which is maintained by randomized outbreeding among 175 mating
93 pairs. The result is each individual DO mouse represents a unique combination of
94 segregating alleles drawn from the original eight progenitor lines. The advantages of
95 this outbreeding include normal levels of heterozygosity — similar to the human genetic
96 condition — and substantially increased genetic resolution (CHURCHILL *et al.* 2012). Both
97 the DO mice and their founder progenitor lines have already proven to be successful in
98 identifying genetic associations with intestinal microbiome composition (O'CONNOR *et al.*
99 2014, KEMIS *et al.* 2019).

100 In this study, motivated by the high level of environmental control of the laboratory
101 mouse and the improved mapping resolution of the Diversity Outbred mouse system,
102 we identified genetic underpinnings of the gut microbiota of 247 Diversity Outbred mice.
103 We uncover evidence of host genetic factors influencing the composition of many
104 specific attributes of the gut microbiome (**Figure 1**). These included not only
105 associations between specific host genetic variants and abundances of particular
106 bacterial taxa, but also associations with functional molecular pathways.

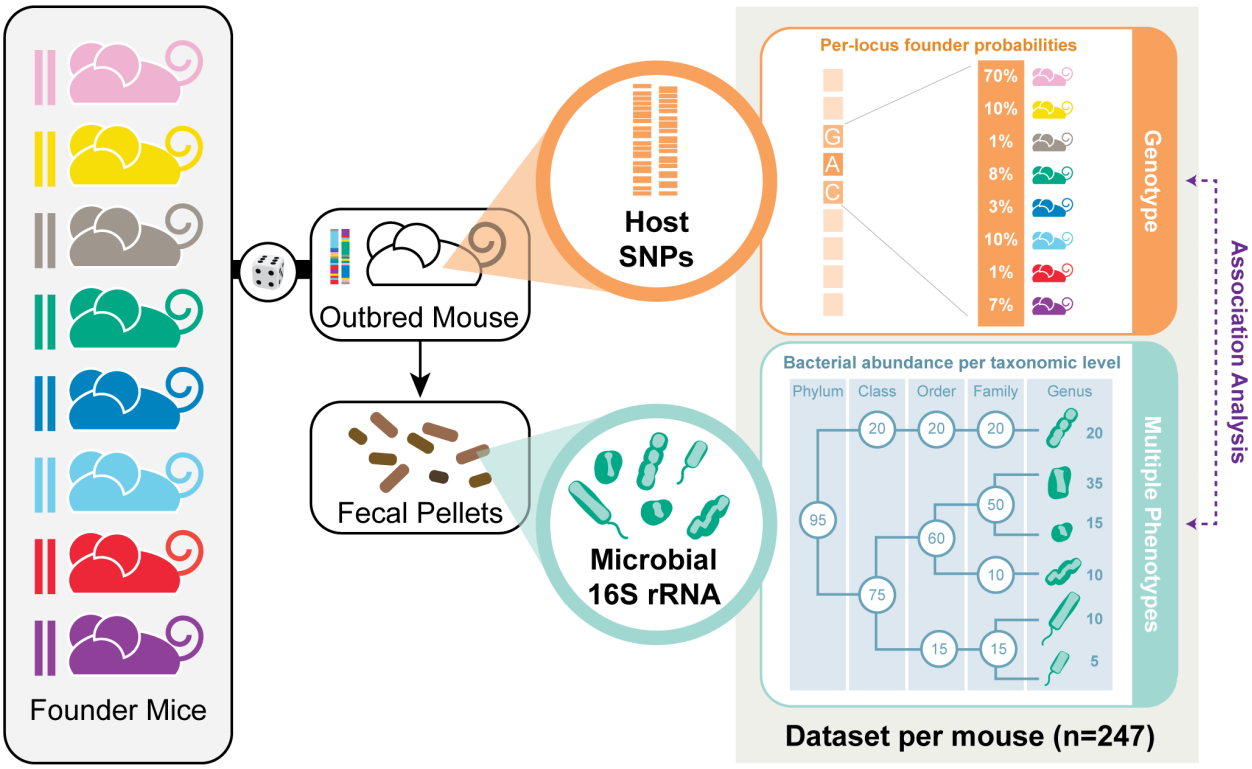

Figure 1. Data flow schematic. Each of the 247 mice in this study represents a unique combination of segregating alleles, whose genome is a unique sampling from the original eight progenitor lines (founder mice). The SNP genotype of each mouse is represented by an eight-founder state probability. Microbial 16S rRNA from fecal pellets from each DO mouse provided bacterial relative abundances, which were aggregated at each taxonomic level and used as separate phenotypes/traits.

113 **MATERIALS AND METHODS**

114 ***Animal population and sample collection***

115 Male mice from the Diversity Outbred Mouse Panel were obtained from The
116 Jackson Laboratory (Bar Harbor, ME, USA) at 6 weeks of age. Experiments were
117 performed at the University of Pennsylvania, Center for Sleep. Mice were group-housed
118 (5 animals per cage) for 2 weeks of post-travel acclimation, and then single-housed at
119 identical conditions with lights on/lights off at 7:00 AM/7:00 PM with a lux level of 60 and
120 temperature 23-25˚C. Bedding used in home cages was Bed-o Cobs 1/8" (The
121 Andersons Inc., Maumee, OH). Mice were fed *ad libitum* Laboratory Autoclavable
122 Rodent Diet 5010 (Lab Diet, St. Louis, MO). Fecal pellets from 249 mice were collected
123 at 3 months old (two samples were later discarded, leaving a final analyzed dataset of
124 247 mice). The pellets were collected from the mouse cage at 10:00 AM, i.e., 3 hours
125 after lights on. Pellets were stored in Eppendorf tubes placed on dry ice and moved to a
126 -80°C freezer until shipping and processing at Cornell University (Ithaca, NY, USA).

127 ***Microbial DNA extraction, 16S rRNA gene PCR, and sequencing***

128 Microbial community DNA was extracted from one single frozen pellet per sample
129 using the MO BIO PowerSoil-htp DNA Isolation Kit (MO BIO Laboratories, Inc., cat #
130 12955-4), but instead of vortexing, samples were placed in a BioSpec 1001 Mini-
131 Beadbeater-96 for 2 minutes. We used 10-50 ng of sample DNA in duplicate 50 µl PCR
132 reactions with 5 PRIME HotMasterMix and 0.1 µM forward and reverse primers. We
133 amplified the V4 region of 16S rRNA gene using the universal primers 515F and
134 barcoded 806R and the PCR program previously described CAPORASO *et al.* (2011), but

135 with 25 cycles. We purified amplicons using the Mag-Bind® E-Z Pure Kit (Omega Bio-
136 tek, cat # M1380) and quantified with Invitrogen Quant-iT™ PicoGreen® dsDNA
137 Reagent, and 100 ng of amplicons from each sample were pooled and paired end
138 sequenced (2x250bp) in two separate sequencing runs on an Illumina MiSeq instrument
139 at Cornell Biotechnology Resource Center Genomics Facility.

140 ***16S data processing***

141 We performed demultiplexing of the 16S rRNA gene sequences and OTU picking
142 using the open source software package Quantitative Insights Into Microbial Ecology
143 (QIIME) version 1.9.0 with default methods (CAPORASO *et al.* 2010). The total number of
144 sequencing reads was 15,149,384, with an average of 61,334 sequences per sample
145 and ranging from 17,658 to 135,803. Open-reference OTU picking at 97% identity was
146 performed against the Greengenes 8_13 database. 12% of sequences failed to map in
147 the first step of closed-reference OTU picking. The taxonomic assignment of the
148 reference sequence was used as the taxonomy for each OTU. 'NR' within taxa names
149 represents New Reference OTUs defined as those with sequences that failed to match
150 the reference and are clustered *de novo*. Random subsamples were used to create a
151 new reference OTU collection and 'NCR' represents New Clean-up Reference OTUs
152 that failed to match the new reference OTU collection (RIDEOUT *et al.* 2014).

153 For the non-rarefied data, read count was used as an additional covariate during
154 QTL mapping to reduce the effect of sequencing depth. A rarefied dataset was also
155 used for heritability estimates and QTL mapping, as explained in **File S1**. Two extreme
156 outliers were omitted from further analysis, yielding a total of 247 samples. To

157 differentiate the non-rarefied taxa from the rarefied taxa, we use 'NonR' to represent the
158 non-rarefied dataset and 'R' to represent the rarefied dataset.

159 For heritability estimates and QTL mapping, a filter was applied across all 247
160 samples that removed any taxon that was not present in more than 50% of the samples.
161 Relative abundance of reads (number of reads clustered to each taxa divided by the
162 total number of reads in a given sample) was used as the tested phenotype. Relative
163 abundances were rank Z-score transformed using R-package *DOQTL* (GATTI *et al.*
164 2014).

165 Stacked bar plots of the most abundant taxa within each taxonomic level were
166 plotted with R-package *ggplot2*. A box-plot was first generated for each taxonomic level
167 depicting the relative abundances of the taxa within that taxonomic level across the 247
168 samples (**Figure S1**). The top ten taxa with the highest average relative abundances
169 are selected to be plotted in the stacked bar plot, ordered by the most abundant taxon.
170 A heatmap that correlates similarities between taxa from the non-rarefied and rarefied
171 datasets based on the Pearson correlation coefficient was plotted using the R-package
172 *corrplot* (**Figure S3**).

173 ***SNP genotyping***

174 SNP genotyping was done at the Jackson Laboratories on each of the 247 mice
175 using The Mega Mouse Universal Genotyping Array (MegaMUGA). A total of 57,973
176 SNPs passed QC metrics and were used in the heritability and mapping analysis
177 reported here.

178 ***Heritability estimation***

179 Heritabilities of the various bacterial taxa were quantified and calculated on
180 autosomes using a linear mixed model as implemented in R-package *lme4qtl* via the
181 relmatLmer() function (ZIYATDINOV *et al.* 2018) (https://github.com/variani/lme4qtl). This
182 linear mixed model enables us to decompose variability into genetic and environmental
183 components. The variance of the genetic component is expected to be $\sigma_g^2 K$, where K is
184 a kinship matrix normalized as proposed in (KANG *et al.* 2010). The kinship matrix is
185 specified via the "relmat" argument in relmatLmer(). To account for the potentially
186 confounding effects of shared cages during acclimation (as noted above under **Animal**
187 **population and sample collection**), we also included cage as a random effect in our
188 model. Thus, the model included estimates of variance of the genetic component (σ_g^2)
189 and the cage component (σ_{cage}^2), and the residual variance due to unspecified
190 environmental factors (σ_{rs}^2). The narrow sense heritability was then estimated as:

191 $$h^2 = \frac{\sigma_g^2}{\sigma_g^2 + \sigma_{cage}^2 + \sigma_{rs}^2}$$

192 Sequencing run was included as a covariate in both non-rarefied and rarefied
193 datasets. For our non-rarefied dataset, narrow sense heritabilities were calculated using
194 the number of read counts as an additional covariate. Significance of heritability

195 estimates was assessed by conducting a restricted likelihood ratio test using the
196 exactRLRT() function in the R-package *RLRsim* (SCHEIPL *et al.* 2008), as applied in
197 Supplementary Note 3 in ZIYATDINOV *et al.* (2018). We calculated standard errors for the
198 heritability estimates following code posted on the *lme4qtl* GitHub page:
199 https://github.com/variani/lme4qtl/blob/master/demo/se.R. This script uses the
200 deltamethod() function in the R-package *msm* (https://github.com/chjackson/msm) to
201 approximate standard errors using the delta method. Proportion variance estimates for
202 kinship and cage for all taxa and their taxonomic level for rarefied data are presented in
203 **Figure S4**. A comparison of heritability estimates and standard error between non-
204 rarefied and rarefied data can be seen in **Figure S5**.

205 ***QTL Mapping***

206 For QTL mapping, rank Z-score transformed relative abundances were mapped
207 using a linear mixed model in R-package *lme4qtl::relmatLmer()* (ZIYATDINOV *et al.* 2018)
208 (fit using maximum likelihood (ML), REML=F) on autosomes with kinship included as a
209 random effect to account for genetic relatedness among animals. For the bacterial taxa
210 from the five taxonomic levels, we generated QTL mappings with the taxa designated
211 as the phenotype. Sequencing run (fixed effect) and cage (random effect) were included
212 in both non-rarefied and rarefied datasets. We included read count as an additional
213 covariate (fixed effect) for our non-rarefied dataset. Significant and suggestive
214 associations were identified in a two-step procedure. First, we applied likelihood ratio
215 tests comparing models with and without genotype. *P*-values derived from these tests
216 were adjusted for multiple testing across SNPs (within a given taxon) using R function
217 p.adjust() with method “BH” (BENJAMINI AND HOCHBERG 1995). In the second step, we

218 conducted permutation tests (1000 permutations) for taxa that had associations with
219 adjusted *p*-value < 0.1 in the maximum likelihood analysis. Due to the computational
220 cost of performing permutation tests for each taxa/peak combination, we further filtered
221 the permutation candidates by only querying the peak with the lowest likelihood p-value
222 in regions with peak overlaps. This resulted in permutation *p*-values for 4 taxa and 4
223 peaks (**Table 2**). Annotated genes found within QTL regions with permutation *p*-value <
224 0.1 can be found in **Table S5**. Although *p*-values are corrected within each trait, no
225 additional adjustment is made for the search across traits.

226 For every bacterial taxon from the five taxonomic levels with a statistically
227 significant QTL association, we mapped the OTUs belonging to that taxon. We applied
228 a 50% zero cut-off filter to only retain common OTUs and generated QTL mappings and
229 assessed significance as described above for the five taxonomic levels.

230 When necessary for comparison, genomic coordinate spans from other
231 publications were translated from human hg19 assembly to mouse mm10 assembly
232 using LiftOver (UCSC). Particularly in the case of small spans or single nucleotides,
233 LiftOver might require expanding the window being mapped. In our case, we iteratively
234 increased the window by adding a padding of 0, 10,100,1000,10000, and 100000 bps
235 on each side of the region of interest until a mapping was achieved. All mapped entries
236 listed include the final span of the genomic coordinates used including padding (**Table**
237 **S7D**).

238 ***Gene Set Pathway Analysis***

239 We used Ingenuity Pathway Analysis (IPA®, QIAGEN Redwood City, CA) software
240 to conduct gene set pathway analysis on the protein-coding non-predicted genes within
241 our QTL regions. Genes were uploaded as NCBI Gene IDs for ease of mapping across
242 IPA's source databases. All analyses were constrained to consider only direct
243 relationships and exclude any annotation predictions. Additionally, we used IPA's
244 stringent filter to constrain the analysis to Mouse annotation while considering all
245 Tissues and Cell Lines. IPA by default shows uncorrected *p*-values for enrichment
246 analyses. We customized all charts and tables to indicate Benjamini-Hochberg False
247 Discovery Rate instead. In total, we submitted 6 gene lists for parallel analyses, all of
248 which were filtered to exclude predicted genes and non-protein coding genes: (1) all
249 genes within any significant QTL region at any taxonomic level, (2) Bacillales only, (3)
250 Bacteroidales only, (4) Mollicutes only (5) Ruminococcaceae only, and (6)
251 *Staphylococcus* only. Many taxonomic groups result in similar-enough QTLs that their
252 gene sets are identical, these groups are the result of picking the lowest taxon for any
253 identical gene sets while covering all the taxa studied (for instance, phylum Tenericutes
254 is excluded as it matches the results of class Mollicutes).

255 ***Data Availability***

256 Our study was performed on a subset of Diversity Outbred mice from the Allan
257 Pack Sleep Study; the genotypes can be downloaded from the Jackson Lab Diversity
258 Outbred Database (DODB) website (https://dodb.jax.org). QIIME demultiplexed fastq
259 files with microbiome data are available in the NCBI SRA, BioProject ID: PRJNA639769
260 (https://www.ncbi.nlm.nih.gov/bioproject/639769). All Supplemental Materials (**File S1**,

261 **Figures S1-S5**, and **Tables S1-S9**) have been uploaded to GSA FigShare under
262 "Supplemental Material for Schlamp et al., 2020", and a description of each can be
263 found at the end of the manuscript.

264 **RESULTS**

265 ***Variation of gut microbiota***

266 High-throughput sequencing of fecal samples from 247 three month old male mice
267 from the Diversity Outbred Mouse Panel generated 15,149,384 16S rRNA gene
268 sequences that passed the quality filtering criteria after demultiplexing (see **Materials**
269 **and Methods**). On average, 61,334 sequences were obtained per sample (ranging
270 from 17,658 to 135,803 sequences). Sequences were sorted into 57,014 operational
271 taxonomic units (OTUs) at 97% identity against the Greengenes 8_13 database using
272 open-reference OTU picking (**Table S1A**). Next, OTUs were summarized at five levels
273 of taxonomy (phylum, class, order, family, genus) (**Table S2A**). In order to focus on the
274 most abundant microbes, only the taxa present in at least 50% of samples (i.e. present
275 in 124 samples or more) were used for all following analysis, leaving a total of 75 taxa to
276 test at the five levels of taxonomy (6 phyla, 8 classes, 11 orders, 20 families, and 30
277 genera). The most predominant taxa at the phylum level were Firmicutes (average
278 relative abundance = 48.64%) and Bacteroidetes (46.41%), which is consistent with
279 previous findings in mice (BENSON *et al.* 2010; MCKNITE *et al.* 2012; ORG *et al.* 2015).
280 The relative abundances of these taxa were highly variable, with Firmicutes ranging
281 from 11% to 94%, and Bacteroidetes ranging from 1% to 88% (**Figure 2, Figure S1**).

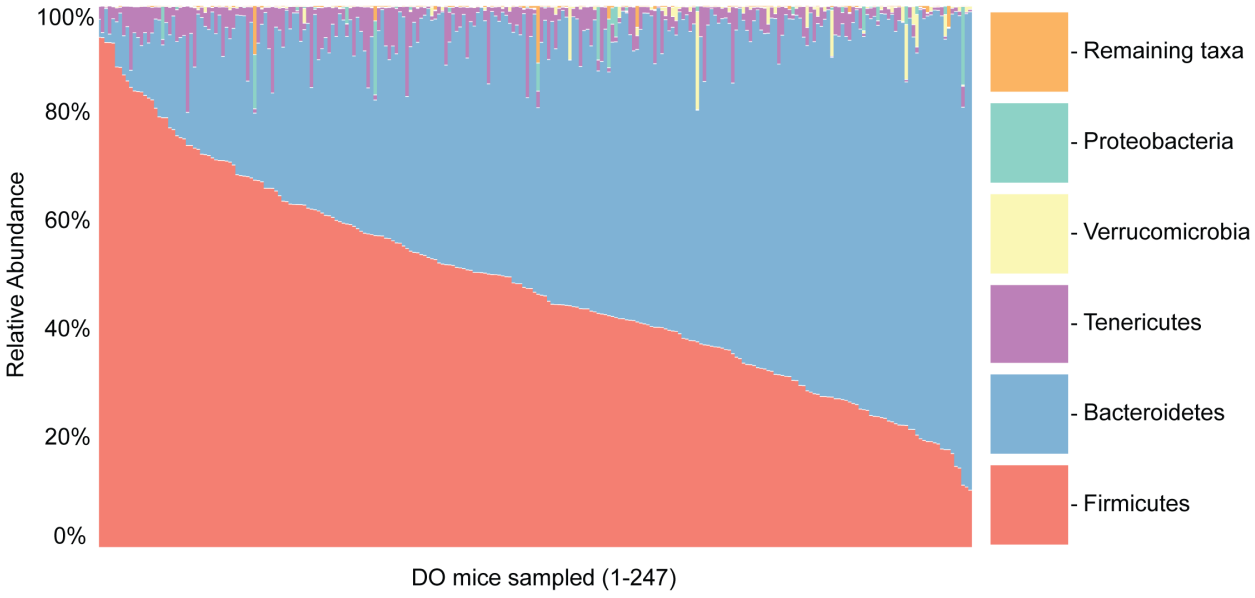

Figure 2. Relative abundances of top ten most abundant phyla across the 247 DO mice. Relative abundances shown, mouse samples sorted by phylum Firmicutes, the most abundant phylum.

The top 8 most abundant genera were present in at least 99% of the samples. The two most abundant genera were an unidentified genus within Bacteroidales family S24-7 (average relative abundance = 43.89%, ranging from 1% to 88%) and another unidentified genus within Clostridiales (32.35%, ranging from 4% to 78%), consistent with previous findings in mice (SHIN *et al.* 2016).

When dealing with uneven sequence counts across samples, microbiome studies commonly normalize the data by rarefying sequence counts, which consists of randomly selecting from each sample an equal number of sequences without replacement (WEISS *et al.* 2017). It has been argued, however, that rarefaction is not an ideal approach due to valuable data being discarded (MCMURDIE AND HOLMES 2014). Therefore, we decided to present our analysis of the non-rarefied data using sequence counts per sample as a covariate, noting also that the rarefied data consisted of highly similar relative

297 abundances, and provided similar heritability and QTL results (see **File S1** for a detailed
298 breakdown of these metrics**).**

299 ***Heritability estimation***

300 Each of the 247 individual DO mice used in this study represents a unique
301 genomic combination of alleles from the original eight progenitor lines. The unit of
302 inference for phenotypes was the rank Z-score transformed relative abundance of each
303 taxon at each taxonomic level (phylum, class, order, family, genus) in each individual
304 mouse, while the units of genetic inference were the SNP genotypes at each of 57,973
305 sites for each mouse using the MegaMUGA mouse genotyping array (**Figure 1**). Each
306 SNP genotype is represented by an eight-founder state probability that corresponds to
307 the probabilities contributed by each founder at each SNP (SVENSON *et al.* 2012) and
308 those eight-founder probabilities are used to fit the linear models (see **Material and**
309 **Methods**).

310 We estimated narrow-sense "SNP" heritability (h^2) using a linear mixed model in R-
311 package *lme4qtl* (ZIYATDINOV *et al.* 2018). A linear mixed model was used to predict
312 whether the effects of the autosomal genotype on the phenotype is proportional to the
313 genetic similarity between the mice, after adjustment for known factors. Thus,
314 calculations were based on the kinship matrix (genetic similarity; also called genetic
315 relatedness matrix (GRM)), expression of a phenotype (taxon relative abundance)
316 across all samples, and additional covariates (such as sequencing run, read counts,
317 and cage effect). Significance was assessed by a restricted likelihood ratio test using R-
318 package *RLRsim* (SCHEIPL *et al.* 2008). More details can be found in **Materials and**
319 **Methods**. Heritability estimates ranged from 0% to 40%. In total, 23 of the 75 tested

320 taxa were significantly heritable (RLRT *p*-value < 0.05); we additionally note multiple-
321 hypothesis normalized Benjamini-Hochberg (BH) False Discovery Rates (**Figure 3**,
322 **Table S3A**). We hypothesized that higher-level taxa would be found to be more
323 heritable than lower level taxa, assuming strong functional relatedness between
324 members of the same taxonomic group, but found that there is no consistent trend
325 between the taxonomy level and heritability. Our most heritable taxon, the class
326 Mollicutes (40%, RLTR *p*-value of 0.0017, BH *p*-value of 0.0884) had a higher
327 heritability estimate than any clade below it (genus *Anaeroplasma* with 29% and an
328 unclassified genus in order RF39 with 35%). In contrast, the heritability estimate of class
329 Bacilli (25%), is surpassed by its subclade, the order Lactobacillales (33%), which is in
330 turn surpassed by its genus *Lactobacillus*, our second most heritable taxon (36%, RLTR
331 *p*-value of 0.0076, BH *p*-value of 0.1035). Proportion variance estimates for kinship and
332 cage for all taxa and their taxonomic level are presented in **Figure 3**.

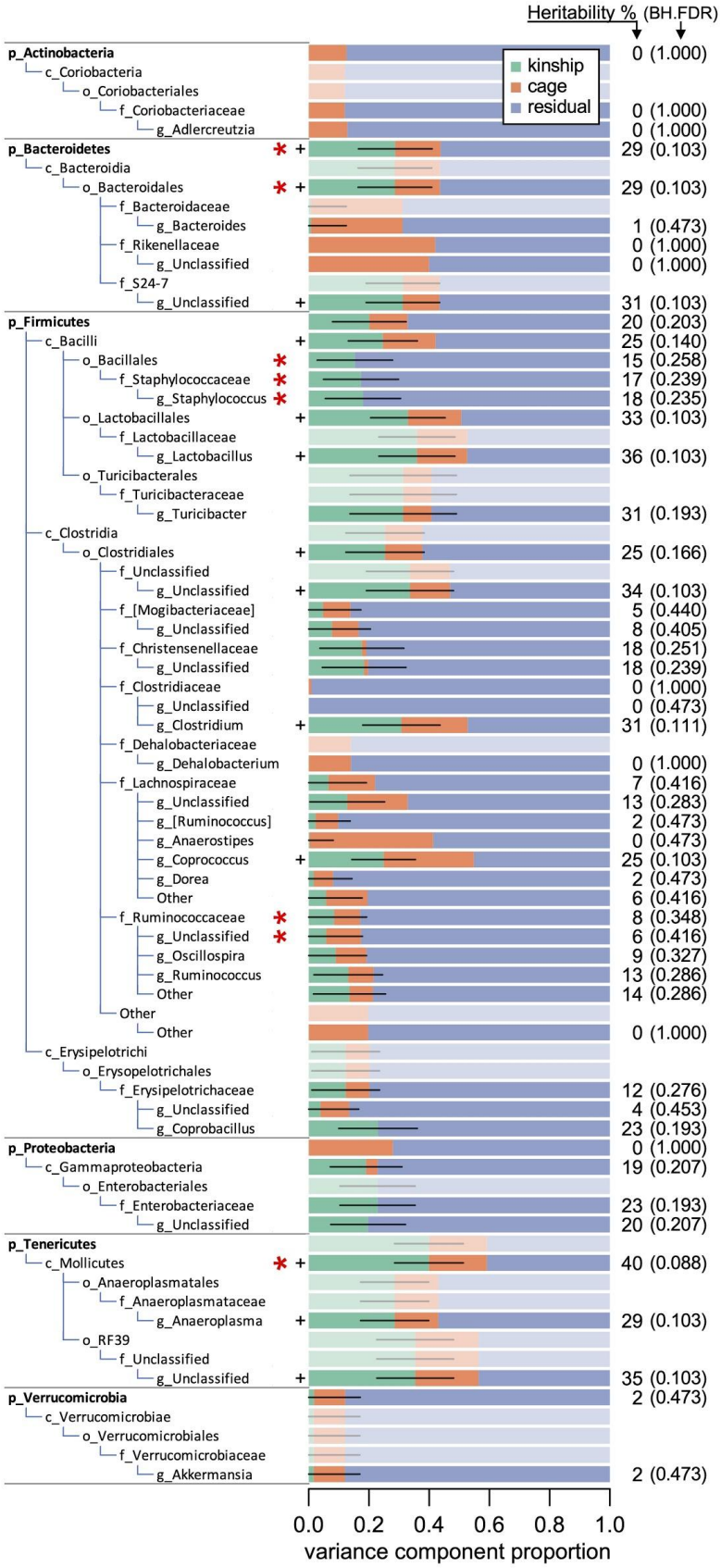
Heritability % (BH.FDR)
kinship
cage
residual
p_Actinobacteria 0 (1.000)
c_Coriobacteria
o_Coriobacteriales
f_Coriobacteriaceae 0 (1.000)
g_Adlercreutzia 0 (1.000)
p_Bacteroidetes * + 29 (0.103)
c_Bacteroidia
o_Bacteroidales * + 29 (0.103)
f_Bacteroidaceae
g_Bacteroides 1 (0.473)
f_Rikenellaceae 0 (1.000)
g_Unclassified 0 (1.000)
f_S24-7
g_Unclassified + 31 (0.103)
p_Firmicutes 20 (0.203)
c_Bacilli + 25 (0.140)
o_Bacillales * 15 (0.258)
f_Staphylococcaceae * 17 (0.239)
g_Staphylococcus * 18 (0.235)
o_Lactobacillales + 33 (0.103)
f_Lactobacillaceae
g_Lactobacillus + 36 (0.103)
o_Turicibacterales
f_Turicibacteraceae
g_Turicibacter 31 (0.193)
c_Clostridia
o_Clostridiales + 25 (0.166)
f_Unclassified
g_Unclassified + 34 (0.103)
f_[Mogibacteriaceae] 5 (0.440)
g_Unclassified 8 (0.405)
f_Christensenellaceae 18 (0.251)
g_Unclassified 18 (0.239)
f_Clostridiaceae 0 (1.000)
g_Unclassified 0 (0.473)
g_Clostridium + 31 (0.111)
f_Dehalobacteriaceae
g_Dehalobacterium 0 (1.000)
f_Lachnospiraceae 7 (0.416)
g_Unclassified 13 (0.283)
g_[Ruminococcus] 2 (0.473)
g_Anaerostipes 0 (0.473)
g_Coprococcus + 25 (0.103)
g_Dorea 2 (0.473)
Other 6 (0.416)
f_Ruminococcaceae * 8 (0.348)
g_Unclassified * 6 (0.416)
g_Oscillospira 9 (0.327)
g_Ruminococcus 13 (0.286)
Other 14 (0.286)
Other
Other 0 (1.000)
c_Erysipelotrichi
o_Erysopelotrichales
f_Erysipelotrichaceae 12 (0.276)
g_Unclassified 4 (0.453)
g_Coprobacillus 23 (0.193)
p_Proteobacteria 0 (1.000)
c_Gammaproteobacteria 19 (0.207)
o_Enterobacteriales
f_Enterobacteriaceae 23 (0.193)
g_Unclassified 20 (0.207)
p_Tenericutes
c_Mollicutes * + 40 (0.088)
o_Anaeroplasmatales
f_Anaeroplasmataceae
g_Anaeroplasma + 29 (0.103)
o_RF39
f_Unclassified
g_Unclassified + 35 (0.103)
p_Verrucomicrobia 2 (0.473)
c_Verrucomicrobiae
o_Verrucomicrobiales
f_Verrucomicrobiaceae
g_Akkermansia 2 (0.473)
0.0 0.2 0.4 0.6 0.8 1.0
variance component proportion

333

334 **Figure 3. Proportion of variance estimates for kinship and cage for all taxa.** Proportion of variance
335 estimates for kinship (green), cage effects (orange), and unexplained residual effects (blue) for each
336 taxon. The kinship proportion of variance is an estimate of narrow sense heritability. Heritability
337 percentages are shown on the left. Heritability standard errors are shown with black horizontal lines.
338 Designations p_, c_, o_, f_, and g_ are for phylum, class, order, family, and genus, respectively. When
339 results are identical across taxa in the same phylogenetic branch, only the lowest (most specific) taxa are
340 shown and the rest are shaded out. Heritability significance is marked with one plus (**+**, RLTR *p*-value <
341 0.05) and BH FDR is shown in parentheses next to heritability percentages. Taxa marked with a red
342 asterisk have statistically suggestive QTL (*, adj. *p*-value < 0.1). Complete table of heritability results,
343 including rarefied data, can be found in **Table S3**.

344 ***QTL Mapping***

345 QTL mapping of the bacterial taxa at the five taxonomic levels revealed findings
346 that suggest statistically significant associations between host genotype and relative
347 abundances of certain taxa. QTL regions on autosomes were found using the R-
348 package *lme4qtl* (ZIYATDINOV *et al.* 2018). Significance was assessed first by
349 comparison of models with and without genotype via a likelihood ratio test, followed by a
350 genome-wide permutation test. The reported *p*-values were corrected for multiple
351 testing across SNPs (but not across taxa). In total, genetic associations with the
352 abundance of family Ruminococcaceae, family Staphylococcaceae, and genus
353 *Staphylococcus* were found to be statistically significant (adj. *p*-value < 0.05), and
354 additional genetic associations with phylum Bacteroidetes, order Bacteroidales, order
355 Bacillales, and class Mollicutes were statistically suggestive (adj. *p*-value < 0.1). QTLs
356 of order Bacteroidales, genus *Staphylococcus*, and family Ruminococcaceae were also
357 statistically suggestive at a permutation *p*-value < 0.1 (**Table S5**).

358 QTL regions are defined by all contiguous SNPs with LODs above significance
359 threshold of adjusted *p*-value < 0.1, as illustrated in **Figure 4C**. Multiple QTL for various
360 taxa overlapped with the QTL regions for their parent taxa, such as a QTL hit for genus
361 *Staphylococcus* (a genus in the family Staphylococcaceae) overlapping the QTL hit for
362 family Staphylococcaceae (**Table 1**). The relationship between loci and microbial
363 abundance is treated as an independent association analysis per taxa. An example of
364 how these parallel analyses detect similar genomic regions across related taxa is further
365 illustrated in **Figure 5**.

366 **Table 1. QTL regions for taxa at five taxonomic levels**. Only showing ranked results with adj. *p*-value <
367 0.1 (statistically suggestive). Results with adj. *p*-value < 0.05 (statistically significant) are bolded. When
368 results were overlapping across taxa in the same phylogenetic branch (such as phylum Bacteroidetes
369 and order Bacteroidales), permutations were calculated only for the lowest (most specific) taxon.
370 Complete table of QTL results, including rarefied data, can be found in **Table S4**.

		chr[a]	maxlod[b]	pos[c]	from[d]	to[e]	*p*-value	adj.*p*-value	perm.*p*-value
Taxa	phylum Bacteroidetes	5	7.65	118.58	117.39	118.82	1.02E-05	0.068	NA
	order Bacteroidales	5	7.67	118.58	117.39	118.82	9.69E-06	0.065	0.042
	order Bacillales	19	8.24	27.02	26.55	27.42	3.12E-06	0.055	NA
		19	6.95	27.82	27.82	27.97	4.02E-05	0.085	NA
	family Staphylococcaceae	**19**	**8.09**	**27.04**	**26.55**	**27.46**	**4.17E-06**	**0.032**	NA
		19	**7.84**	**27.82**	**27.61**	**28.18**	**6.96E-06**	**0.032**	NA
		19	6.58	32.10	31.83	32.22	8.33E-05	0.092	NA
		19	6.45	32.43	32.43	32.43	1.07E-04	0.098	NA
	genus *Staphylococcus*	**19**	**8.26**	**27.04**	**26.51**	**27.46**	**3.00E-06**	**0.025**	**0.019**
		19	**7.93**	**27.82**	**27.61**	**28.20**	**5.78E-06**	**0.025**	**0.033**
		19	6.64	32.10	31.83	32.22	7.39E-05	0.082	0.271
		19	6.53	32.43	32.43	32.46	9.14E-05	0.082	0.304
	family Ruminococcaceae	**2**	**7.01**	**170.57**	**170.51**	**170.66**	**3.63E-05**	**0.039**	**0.137**
		2	6.30	170.71	170.71	170.71	1.44E-04	0.100	0.427
		5	**7.18**	**31.93**	**31.77**	**32.19**	**2.59E-05**	**0.035**	**0.106**
		5	**7.44**	**32.52**	**32.27**	**33.36**	**1.55E-05**	**0.035**	**0.066**
	Unclassified genus in family Ruminococcaceae	2	7.89	170.56	170.51	170.64	6.22E-06	0.090	NA
	class Mollicutes	1	7.00	121.32	120.23	125.20	3.66E-05	0.089	0.142

[a] Chromosome in which lies the QTL
[b] Maximum LOD score within the QTL
[c] Position in the chromosome (Mbp) where the maximum LOD score is found
[d] Chromosomal position (Mbp) where the QTL begins
[e] Chromosomal position (Mbp) where the QTL ends

371

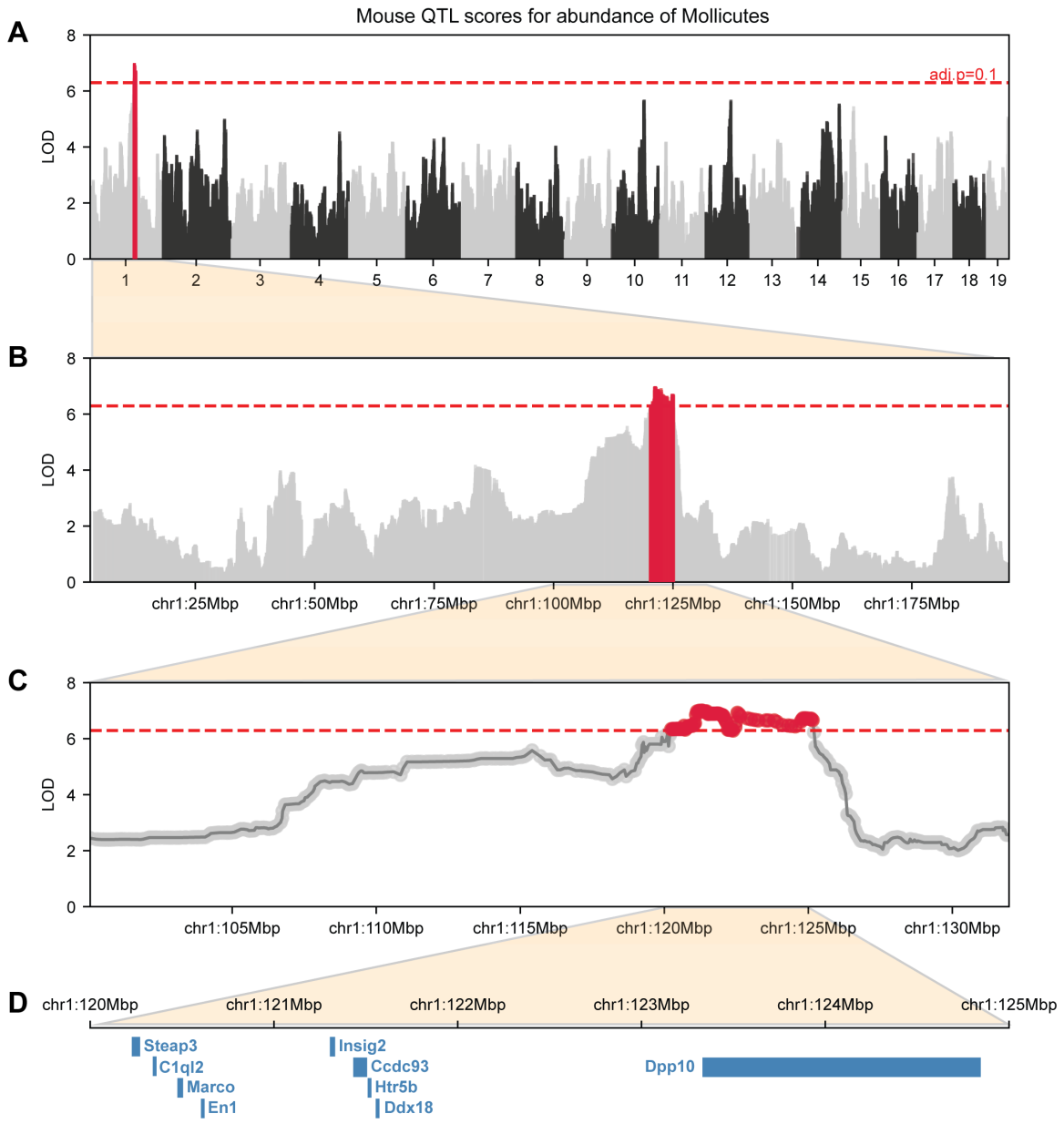

Figure 4. QTL scores for abundance of class Mollicutes. (A) LOD score profile of genome-wide QTL mapping for relative abundance of class Mollicutes shows a significant QTL region (in red) on chr1. Horizontal axis shows genome physical location by chromosome, vertical axis shows LOD score at each site. Horizontal dashed red line marks the significance threshold at adjusted *p*-value < 0.1. (**B**) Chr1 zoomed in shows the significant QTL region in red (chr1:120.24-125.15 Mbp). (**C**) Further zoom into the area of interest shows in clearer detail how the QTL region is determined by a collection of contiguous significant SNPs (above significance threshold). (**D**) *Mus musculus* protein-coding genes within the QTL region are colored in blue.

381 ***OTU level analysis***

382 Next, we decided to increase the specificity of the taxonomic classifications to
383 operational taxonomic units (OTUs) by compiling all OTUs identified within taxa that had
384 statistically suggestive QTL (**Table 1**). We filtered out OTUs that were present in less
385 than 50% of the samples, resulting in 362 OTUs. QTL mapping performed on these
386 selected OTUs resulted in 28 OTUs with at least one statistically significant association
387 (adj. *p*-value < 0.05), and 33 additional OTUs with at least one statistically suggestive
388 association (adj. *p*-value < 0.1) (**Table S6**).

389 QTL associations to OTUs sometimes overlapped with QTL regions associated to
390 taxa at higher taxonomic levels, with the most significant ones corresponding to wider
391 QTL regions (**Table 2**). These results are interesting because if the overlapping QTL
392 region associated with the broader taxonomic group is narrower and more specific than
393 the region seen on an individual OTU, this might suggest a cumulative effect of multiple
394 sub-taxonomies driving a stronger signal at the broader taxonomic level. For example,
395 QTL for OTU 338796 (chr2:169.64-171.00Mbp) and NCR OTU 170146 (chr5:32.27-
396 35.85Mbp) within family Ruminococcaceae were both statistically significant (**Table 2**)
397 and overlapped with QTL regions for Ruminococcaceae (chr2:170.51-170.66Mbp and
398 chr5:32.27-33.36Mbp, respectively) (**Table 1**), but the QTL regions for the OTUs were
399 both wider, as shown in **Figure 5**. Note that factors such as the local recombination
400 intensity profile and SNP density will affect the width of the QTL regions equally across
401 taxonomies, since the relative abundance of each taxon at each taxonomic level is
402 considered as a single phenotype queried against the same static, underlying set of
403 SNPs.

404 **Table 2. QTL regions for OTUs**. Only showing OTUs with adj. *p*-value < 0.1 (statistically suggestive) and
405 with a QTL region overlapping QTL from higher-level taxonomies. Results with adj. *p*-value < 0.05
406 (statistically significant) are bolded. Permutations were calculated only for peaks with the lowest likelihood
407 *p*-value in regions with peak overlaps. OTU numbers are assigned by Greengenes database, 'NR'
408 prefixes denote "New Reference" OTUs defined as those with sequences that failed to match the
409 reference and are clustered *de novo*. 'NCR' prefixes denote "New Clean-up Reference" OTUs that failed
410 to match the new reference OTU collection and are assigned a new random number. Complete table of
411 QTL results for OTUs can be found in **Tables S6**.

		chr[a]	maxlod[b]	pos[c]	from[d]	to[e]	*p*-value	adj.*p*-value	perm.*p*-value
Taxa	OTU 421792 (order Bacteroidales)	5	5.52	118.69	118.67	118.79	6.36E-04	0.088	NA
	OTU 460953 (order Bacteroidales)	5	5.71	118.67	118.63	118.74	4.49E-04	0.085	NA
	OTU 190835 (order Bacteroidales)	5	5.52	118.67	118.67	118.69	6.35E-04	0.090	NA
	OTU 209408 (order Bacteroidales)	5	6.84	118.67	118.52	118.82	5.02E-05	0.066	0.195
	OTU NR.OTU100 (family Ruminococcaceae)	5	8.35	31.93	30.25	32.10	2.46E-06	0.052	0.015
	OTU 338796 (family Ruminococcaceae)	**2**	**8.28**	**170.56**	**169.64**	**171.00**	**2.84E-06**	**0.032**	**0.019**
	OTU NR.OTU95 (family Ruminococcaceae)	5	7.65	31.83	31.30	32.00	1.01E-05	0.065	NA
		5	7.45	32.27	32.11	32.39	1.51E-05	0.065	NA
	OTU 336810 (family Ruminococcaceae)	2	6.47	170.54	170.27	170.59	1.03E-04	0.093	NA
	OTU NCR.OTU170146 (family Ruminococcaceae)	**5**	**7.68**	**33.33**	**32.27**	**35.85**	**9.58E-06**	**0.026**	**0.056**

[a] Chromosome in which lies the QTL
[b] Maximum LOD score within the QTL
[c] Position in the chromosome (Mbp) where the maximum LOD score is found
[d] Chromosomal position (Mbp) where the QTL begins
[e] Chromosomal position (Mbp) where the QTL ends

412

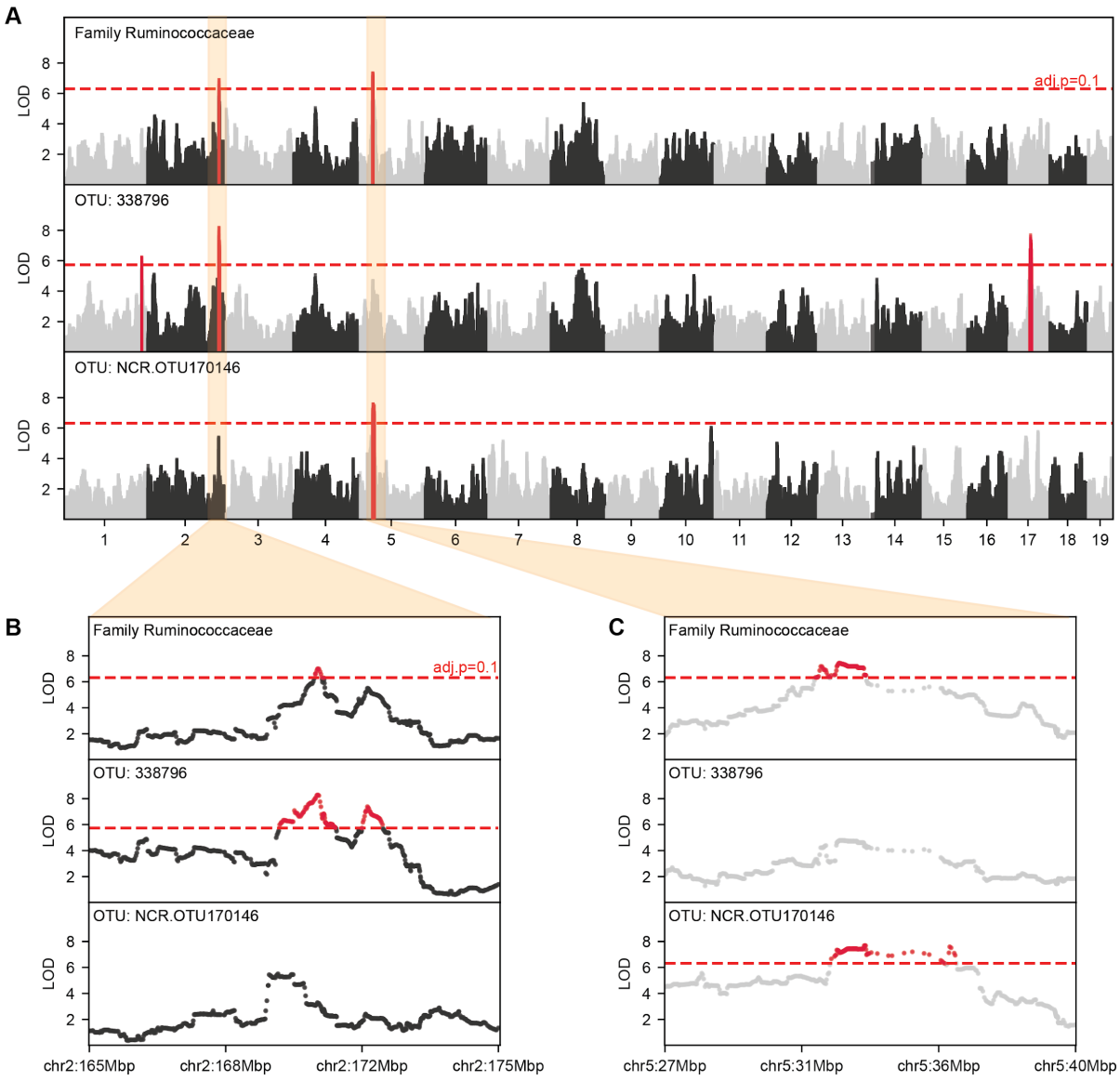

Figure 5. Overlap of QTL regions across taxa in the same phylogenetic branch. (**A**) LOD score profile of genome-wide QTL mapping for relative abundance family Ruminococcaceae (top panel), and two OTUs found within family Ruminococcaceae: OTU 338796 (middle panel), and NCR OTU 170146 (bottom panel). (**B**) Zoom into the area of interest in chr2 shows overlap in QTL regions between family Ruminococcaceae (170.51-170.66Mbp, top panel) and OTU 338796 (169.64-171.00Mbp, middle panel). (**C**) Zoom into the area of interest in chr5 shows overlap in QTL regions between family Ruminococcaceae (32.27-33.36Mbp, top panel) and NCR OTU 170146 (32.27-35.85Mbp, bottom panel). Horizontal axis shows genome physical location by chromosome, vertical axis shows LOD score at each site. Horizontal dashed red line marks the significance threshold at adjusted *p*-value < 0.1.

423 ***Comparison to other studies***

424 Results from other published studies on heritabilities of the various bacterial taxa in
425 the gut microbiome of mice, pigs, and humans were compiled and compared with our
426 results (**Figure 6, Table S7**). We find new evidence of heritability of bacterial taxa in
427 mice only previously seen in human studies. For example, we observed significant
428 heritability in the phylum Tenericutes as well as several of its subclades, including
429 genus *Anaeroplasma* and order RF39. These results were consistent across both our
430 rarefied and non-rarefied datasets, and had not been seen in any other mouse studies,
431 either because they did not detect these taxa in their studies or their results failed to
432 identify significant heritability. This novel result is similar to previous host-microbe
433 associations seen in human studies where significant heritabilities for this taxonomic
434 lineage were identified in phylum Tenericutes (h^2 = 0.34 (GOODRICH *et al.* 2016) and
435 0.23 (LIM *et al.* 2017)), class Mollicutes (h^2 = 0.32 (GOODRICH *et al.* 2016) and 0.23 (LIM
436 *et al.* 2017)), and order *RF39* (h^2 = 0.31 (GOODRICH *et al.* 2016)).

437 In some instances, taxa that we did not identify as being significantly heritable —
438 and in fact have some of our lowest heritability scores — are reported to have high
439 heritability in other studies. We show some examples of this in **Figure 6**: families
440 Clostridiaceae and Lachnospiraceae as well as the entire phylum Verrucomicrobia.
441 Interestingly, both of these families have significantly heritable subclades, whereas the
442 entire branch of phylum Verrucomicrobia had low heritability estimates. We see a very
443 low heritability estimate in both our non-rarefied and rarefied datasets for the genus
444 *Akkermansia* (h^2 = 0.02) and every taxonomic level up to phylum Verrucomicrobia, yet
445 estimates for mice in other studies were as high as h^2 = 0.92 (ORG *et al.* 2015), and h^2 =

0.62 (O'CONNOR *et al.* 2014). This discrepancy between heritability estimates for *Akkermansia* is not mouse specific, as human microbiome studies see similarly conflicting results in their heritability estimates for this same genus: Reporting significantly high (h^2 = 0.30 (TURPIN *et al.* 2016)), significantly low (h^2 = 0.14 (GOODRICH *et al.* 2016)), and close to zero and not significant estimates (h^2 = 0, 0.01 (DAVENPORT *et al.* 2015), and 0.06 (LIM *et al.* 2017)).

	Heritability																
	Mouse								Human								Pigs
	Schlamp '20		Org					O'Connor	Goodrich	Davenport			Turpin	Lim	Hughes		Camarinha-
	nonR	R	All	M	F	Avg	One		'16	W	S	C			HB	RNT	Silva
p_Bacteroidetes	**0.29**	**0.28**	0.53	0.82	0.73	0.00	0.02		0.08				**0.33**	**0.25**			0.20
c_Bacteroidia	**0.29**	**0.28**	0.53	0.82	0.73	0.00	0.02		0.08				**0.33**				0.20
o_Bacteroidales	**0.29**	**0.28**	0.53	0.82	0.73	0.00	0.02		0.08		0.00	0.00	**0.33**	**0.25**		0.00	0.00
f_S24-7	**0.31**	**0.31**	0.60	0.86	0.82	0.00	0.00						**0.33**				
p_Firmicutes	0.20	0.18	0.56	0.71	0.77	0.15	0.16		0.00	0.00	0.00	0.00	0.18	0.10		0.00	
c_Bacilli	**0.25**	**0.24**	0.68	0.74	0.76	0.01	0.00		0.03				0.19	**0.35**			
o_Lactobacillales	**0.33**	**0.35**	0.77	0.79	0.55	0.00	0.00		0.00				0.10	**0.33**	0.09	0.01	
f_Lactobacillaceae	**0.36**	**0.37**							0.04		0.13		**0.26**	**0.17**			0.00
g_*Lactobacillus*	**0.36**	**0.37**						0.74	0.04	**0.36**	0.00	0.19	**0.26**	**0.15**	0.00	0.03	**0.34**
o_Turicibacterales	0.31		0.54	0.75	0.82	0.12	0.12		**0.39**				**0.26**				
f_Turicibacteraceae	0.31		0.54	0.75	0.82	0.12	0.12		**0.39**				**0.26**				
g_*Turicibacter*	0.31		0.54	0.75	0.82	0.12	0.12	0.29	**0.39**	0.00	0.19	0.13	**0.26**				0.00
c_Clostridia	**0.25**	0.24	0.58	0.80	0.77	0.00	0.03		0.03				0.22	0.07			0.00
o_Clostridiales	**0.25**	0.24	0.58	0.80	0.77	0.00	0.03		0.03	0.00	0.00	0.00	**0.33**	0.07		0.03	0.00
f_Christensenellaceae	0.18	**0.33**							**0.42**				**0.64**	**0.31**			
f_Clostridiaceae	0.00	0.00	0.61	0.83	0.80	0.09	0.05		**0.30**	**0.35**		0.00	**0.35**	**0.34**			
g_*Clostridium*	**0.31**								**0.24**	0.10	**0.46**	0.04	0.20	0.14			0.10
f_Lachnospiraceae	0.07	0.08	0.52	0.60	0.69	0.36	0.07		0.16	0.13	0.00	**0.29**	0.17	**0.15**		0.02	0.09
g_*Coprococcus*	**0.25**	**0.29**	0.28	0.61	0.55	0.00	0.02	0.19	0.09	**0.46**	0.06	**0.26**	0.04	**0.16**	0.03	0.13	
p_Tenericutes	**0.40**	**0.36**							**0.34**				0.06	**0.23**			
c_Mollicutes	**0.40**	**0.36**							**0.32**				0.18	**0.23**			
o_Anaeroplasmatales	**0.29**	**0.28**															
f_Anaeroplasmataceae	**0.29**	**0.28**															
g_*Anaeroplasma*	**0.29**	**0.28**						0.48									
o_RF39	**0.35**	**0.32**							**0.31**				0.18				
p_Verrucomicrobia	0.02	0.11	0.54	0.85	0.92	0.13	0.33		**0.15**				**0.30**	0.05			
c_Verrucomicrobiae	0.02	0.11	0.54	0.85	0.92	0.13	0.33		**0.14**				**0.30**				
o_Verrucomicrobiales	0.02	0.11	0.54	0.85	0.92	0.13	0.33		**0.14**				**0.30**				
f_Verrucomicrobiaceae	0.02	0.11	0.54	0.85	0.92	0.13	0.33		**0.14**				**0.30**	0.06			
g_*Akkermansia*	0.02	0.11	0.54	0.85	0.92	0.13	0.33	0.62	**0.14**	0.00	0.01	0.00	**0.30**	0.06	0.14	0.00	
minimum heritability measurement	0.00	0.00	0.26	0.57	0.45	0.00	0.00	0.19	0.00	0.00	0.00	0.00	0.00	0.01	0.00	0.00	0.00
maximum heritability measurement	0.40	0.37	0.77	0.86	0.93	0.36	0.33	0.76	0.42	0.46	0.46	0.37	0.64	0.46	0.22	0.33	0.34

Figure 6. Comparison of taxon heritabilities across mouse, human, and pig studies. The green shading over heritability estimates ranges from each study's lowest heritability estimate (white) to each study's highest heritability estimate (green) to highlight the relative heritability of each taxa per study. Statistically significant results are shown in bold font when significance is reported. For our Diversity Outbred study, we report both non-rarefied (nonR) and rarefied (R) results. For ORG *et al.* (2015) we

458 report results using all mice (All), just males (M), just females (F), an average per strain (Avg), and a
459 single mouse per strain (One). ORG *et al.* (2015) and O'CONNOR *et al.* (2014) did not report significances.
460 For GOODRICH *et al.* (2016) the estimates are calculated by the ACE model, bold values indicate
461 estimates with a 95% confidence interval not overlapping 0. For DAVENPORT *et al.* (2015) the estimates
462 are the proportion of variance explained (PVE) estimates ("chip heritability"), we report winter (W),
463 summer (S), and combined seasons (C) datasets, and bold values indicate estimates with a standard
464 error not overlapping 0. For TURPIN *et al.* (2016) and LIM *et al.* (2017) estimates are polygenic heritability
465 (H2r). For CAMARINHA-SILVA *et al.* (2017) and HUGHES *et al.* (2020) estimates are narrow-sense heritability
466 (h^2). Grey indicates that the taxon was not observed or excluded in a given study. Figure adapted from
467 GOODRICH *et al.* (2016). Comparisons relevant to the text are shown here, with the full comparison found
468 in **Table S7**.

469 In addition to comparing our heritability estimates with other studies, we also
470 contrasted our QTL mapping results of the gut microbiome with those from previous
471 QTL and GWA studies (**Figure 7, Table S7**).

472 We identified statistically significant QTL associations for the order Bacillales as
473 well as for the family Staphylococcaceae and the genus *Staphylococcus* within
474 Bacillales in chr19; another mouse study also found statistically significant QTL
475 associations for all of the same taxa but on chr17 (MCKNITE *et al.* 2012). A human
476 microbiome study found statistically significant QTL regions for the class Bacilli, which
477 comprise the above mentioned order and families (BLEKHMAN *et al.* 2015).

478 Family Ruminococcaceae has been previously found to have significant QTL
479 associations both in mice (chr12 (BENSON *et al.* 2010) and 3 (BELHEOUANE *et al.* 2017))
480 and humans (BLEKHMAN *et al.* 2015, HUGHES *et al.* 2020). In our study,
481 Ruminococcaceae was identified as associated with chromosomes 2 and 5. We also

482 identified a QTL hit for the phylum Bacteroidetes in chr5 while another mouse study
483 identified a significant hit in chr14 (WANG *et al.* 2015). Within Bacteroidetes, even
484 though we did not find any significant QTL results for the genus *Bacteroides*, many
485 other mouse studies have (chr1 (WANG *et al.* 2015, BELHEOUANE *et al.* 2017), 4
486 (MCKNITE *et al.* 2012), 9 (LEAMY *et al.* 2014), 11 (BUBIER *et al.* 2018), 16 (LEAMY *et al.*
487 2014), and 18 (LEAMY *et al.* 2014)) as well as a human study (BLEKHMAN *et al.* 2015).

488 Phylum Tenericutes had a significant hit in chr1 in both our non-rarefied and
489 rarefied datasets, and family Lachnospiraceae had a statistically suggestive QTL in
490 chr10 in our rarefied dataset but not in our non-rarefied dataset. Both of these taxa had
491 significant QTL hits in a human study (BLEKHMAN *et al.* 2015).

492 Finally, we did not observe any QTL overlaps with KEMIS *et al.* (2019) (**Table S7**),
493 which also used the Diversity Outbred mice population in their microbiome association
494 study. This lack of overlap is likely due to the highly different diet used in their
495 experiments (high-fat, high-sucrose), and further highlights the strong impact of diet
496 alone in microbiome composition.

	QTL/GWAS signals										
	Mouse									Human	
	Schlamp '20 nonR	Schlamp '20 R	Benson	McKnite	Leamy	Wang '15 H	Bubier	Belheouane	Kemis	Blekhman	Hughes RNT
p_Bacteroidetes	5	5				14					
c_Bacteroidia											
o_Bacteroidales	5	5									
f_Bacteroidaceae											
g_Bacteroides				4	9,16,18	1	11	1		9 (4)	
p_Firmicutes											1 (3)
c_Bacilli										2 (12), 10 (7), 14 (12)	
o_Bacillales	19			17							
f_Staphylococcaceae	19			17							
g_Staphylococcus	19			17							
c_Clostridia											
o_Clostridiales											1 (3), 11 (9)
f_Lachnospiraceae		10								1 (1)	3 (3)
f_Ruminococcaceae	2,5	2,5	12					3		10 (10)	7 (9)
p_Tenericutes										6 (17)	
c_Mollicutes	1	1									

Figure 7. Comparison of taxa with QTL associations across mouse and human studies. Associations with each taxon are marked in dark blue if statistically suggestive and bolded in white if statistically significant, or light blue if not significant. Gray indicates that the taxon was not observed or excluded in a given study. The chromosome numbers where the QTL were found are denoted in each box. For our Diversity Outbred study, we report both non-rarefied (nonR) and rarefied (R) results. In the human studies, the corresponding syntenic mouse chromosome was added in parenthesis. Figure adapted from GOODRICH *et al.* (2016). Selected comparisons shown, full comparison found in **Table S7**.

Gene level analysis

Examining the QTL mapping results from previous studies, it was apparent that although different studies might all have found significant QTL regions for a particular bacterial taxon, they identified different genomic positions as showing associations. In order to identify common functions and diseases associated with the genes within our QTL regions, we used Ingenuity Pathway Analysis (IPA®, QIAGEN Redwood City, CA) to run a cumulative gene set enrichment analysis on all 1423 genes associated with non-rarefied microbiome abundance spanning 7 significant QTL and 11 suggestive QTL across the five taxonomic levels (phylum, class, order, family, genus) (**Table S4**) and 54

514 significant QTL and 232 suggestive QTL at the OTU level (**Table S6**). All genes found
515 within each QTL region were included. When QTL regions overlapped across taxa of
516 the same phylogenetic branch (as illustrated in **Figure 5**), overlapping genes were only
517 counted once. Additionally, we ran taxon-specific enrichment analysis to profile the
518 specific functions and diseases associated with genes in the QTL regions associated
519 with relative abundance of phylum Firmicutes (n = 23 genes), class Mollicutes (n = 9),
520 order Bacteroidales (n = 10), family Ruminococcaceae (n = 15), and genus
521 *Staphylococcus* (n = 8), excluding OTU-specific QTL regions.

522 Through the cumulative gene set analysis, we found 25 networks each containing
523 subsets of our genes. We can try to characterize the biological significance of these
524 networks by measuring the enrichment of disease and functional annotations in the
525 genes of each network (**Table S8**). We find remarkable functional signatures in the
526 highest-ranked of these 25 networks, with enrichment in the broad categories of
527 Immunological Disease and Inflammatory Response (Network 1, **Figure 8A**), Lipid
528 Metabolism and Molecular Transport (Network 2, **Figure 8B**), and Connective Tissue
529 Development and Function (Network 3, **Figure 8C**). These associations are highly
530 concordant with increasingly well-understood roles in host-microbiome interaction
531 studies. In Network 1, we find the most enriched specific functions relate to microbiome
532 associated phenotypes, namely hypersensitive reactions (BH-FDR = 7.56e-4), allergies
533 (BH-FDR = 1.39e-3), and atopic dermatitis (BH-FDR = 6.35e-3). Additionally, we find
534 that despite lack of overlap between the gene membership of these four highest-ranked
535 networks, they all have a significant enrichment for functions in both Gastrointestinal
536 Disease (BH-FDRs between 1.26e-3 and 2.47e-3) and Digestive System Development

537 and Function (BH-FDRs between 3.41e-3 and 3.34e-2). Interestingly, we also find
538 consistent significant enrichment of cancer annotations across all four networks with
539 varying overlap of tissues: prostate and renal cancers (Network 1), metastasis and
540 colorectal cancer (Network 2), and breast, ovarian, and gastrointestinal cancer (Network
541 3). Only liver cancer appeared to be enriched in all three networks. A full exhaustive list
542 of significantly enriched categories, diseases, and functions can be found in **Table S9**.

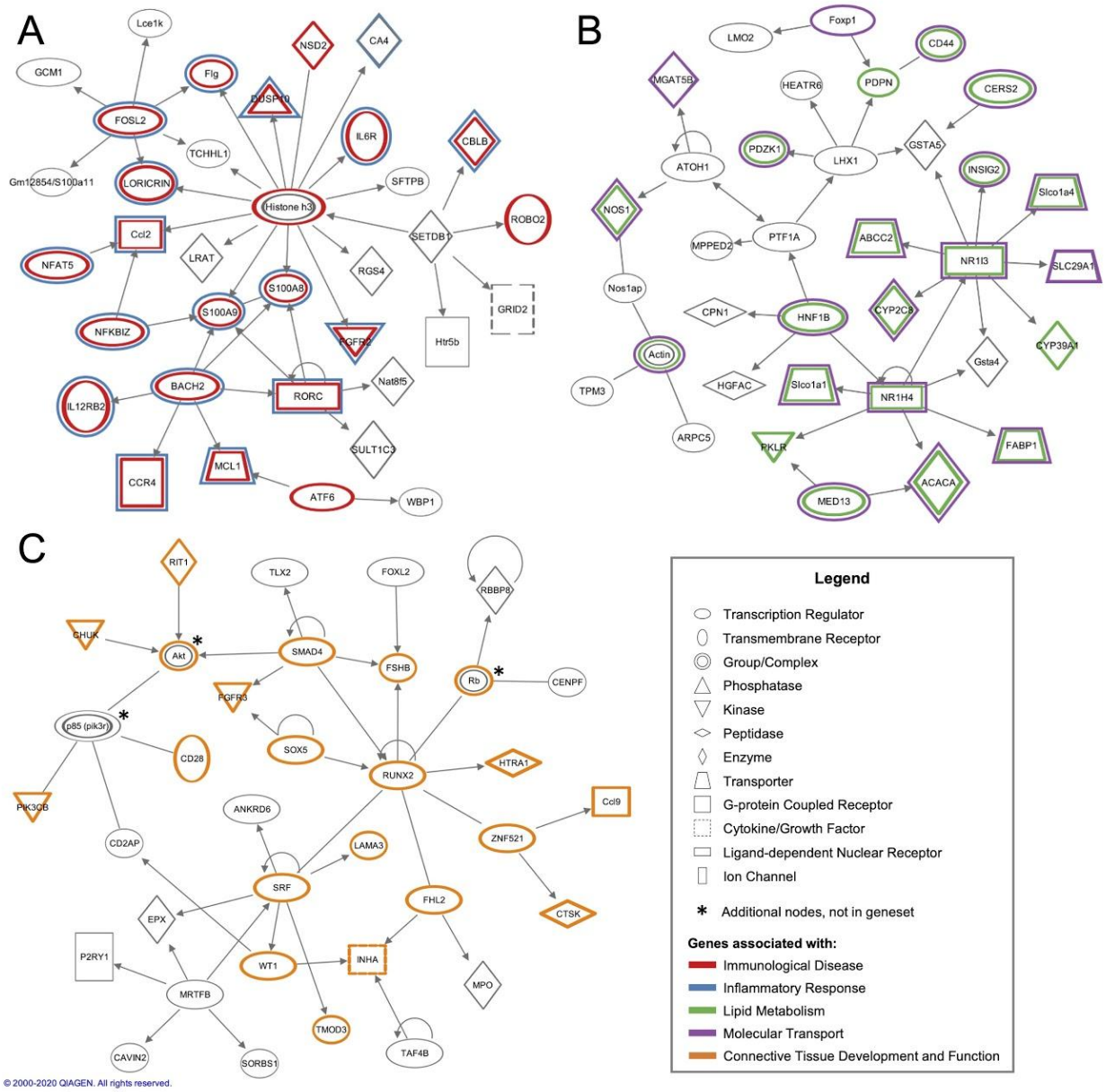

Figure 8. Ingenuity Pathway Analysis (IPA) three highest-ranked interaction networks generated from cumulative gene set analysis. Genes circled in color are all associated with disease and functional annotations as specified below. Nodes marked with an asterix belong to closely associated genes added by IPA that were not in the input dataset. (**A**) Network 1 shows genes associated with Immunological Disease (circled in red) and Inflammatory Response (blue). (**B**) Network 2 shows genes associated with Lipid Metabolism (green) and Molecular Transport (purple). (**C**) Network 3 shows genes associated with Connective Tissue Development and Function (orange).

551 Through taxon-specific enrichment analysis we find a consistent enrichment in
552 development of adenocarcinoma (FDRs between 0.00% and 2.87%) in what are
553 otherwise heterogeneous functional profiles (**Figure S2A-E**). We observe an
554 enrichment of lipid metabolism pathway annotation through genes ASAH2, VLDLR, and
555 SGMS1 in the phylum Firmicutes (FDRs 0.31% to 2.73%) all of which are again
556 detected in its subclade, the genus *Staphylococcus* (FDRs 0.22% to 2.98%) (**Figure**
557 **S2A,B**). We also observe an enrichment in breast and ovarian cancer annotations in
558 phylum Firmicutes (FDRs 0.31% to 2.73%), which is shared with its larger subclade, the
559 family Ruminococcaceae (FDRs 0.34% to 2.95%) (**Figure S2A,C**).

560 Finally, in both the cumulative and taxon-specific gene sets we find genes
561 canonically tied to the commensal microbiome and pathogen-host interactions. The
562 gene MARCO, which lies within a QTL for the abundance of class Mollicutes, encodes a
563 pattern recognition receptor which is part of the innate antimicrobial immune system,
564 binding both Gram-positive and Gram-negative bacteria. We consistently find genes
565 associated with bacterial response in these gene sets, including TLR2, a membrane
566 protein that recognizes bacterial, fungal and viral molecules and has been shown to
567 have benign associations when binding a protein produced by the gut microbiome
568 (OTTMAN *et al.* 2017). These gene sets also include both FCGR1A and FCER1G,
569 fragments of the high affinity IgE Receptor, Spondin2, a cell adhesion protein that binds
570 directly to bacteria and their components as an opsonin for the macrophage
571 phagocytosis of bacteria, BPIFA1, an antimicrobial protein that inhibits the formation of
572 biofilm by Gram negative bacteria, and both PGLYRP3 and PGLYRP4, both

573 peptidoglycan recognition proteins that bind to murein peptidoglycan of Gram-positive
574 bacteria.

575 **DISCUSSION**

576 There exists a complex and multifaceted relationship between the gut microbiome
577 and its host's genome, where recent studies are beginning to show the true magnitude
578 of these connections. Our results seek to further understand this relationship by
579 measuring the heritability of bacterial relative abundance phenotypes and by
580 categorizing the functional and disease pathways that may be associated with specific
581 bacterial abundances in the mouse gut microbiome.

582 We detect the first instance of statistically significant heritability in the phylum
583 Tenericutes in a mouse model. Specifically, we see that its subclade, class Mollicutes,
584 is our most heritable taxon (40% BH *p*-value of 0.088). Dramatic increases in Mollicute
585 abundance have been observed in mice when subjected to a high-fat, high-sugar diet in
586 comparison to a plant polysaccharide-rich diet. This Mollicute bloom seems to come at
587 the expense of Bacteroidetes abundance and an overall lower diversity in murine
588 microbiomes (TURNBAUGH *et al.* 2017). Understanding the heritable aspects of Mollicute
589 abundance could help elucidate the host-genetic determinants of body weight control
590 and the etiology of obesity, which has been thus far extremely challenging with host-
591 genome GWAS alone (MÜLLER *et al.* 2018, SPEAKMAN et al. 2018).

592 Our second most heritable taxon is genus *Lactobacillus* (36% BH *p*-value of
593 0.103), which shares a similarly strong but benign association to body weight control in
594 the literature. The genus *Lactobacillus* contains several species with strains commonly

595 used as probiotics. In contrast to the Mollicute lineage, *Lactobacilli* have been used in
596 mouse models of hyperlipidemia to show an increase of abundance of Bacteroidetes
597 and Verrucomicrobia, and improving their lipid metabolism (CHEN *et al.* 2014). The
598 function of these clades as a whole is, however, not clear-cut: *Lactobacillus* is a large
599 genus containing species and strains with differing roles and probiotic effects in humans
600 (MCFARLAND *et al.* 2018) and members of the class Mollicutes may have strain-specific
601 positive effects on gastrointestinal disease in mice, rather than a negative phenotype as
602 a whole (ZHAI *et al.* 2019).

603 These examples present a microbiome-host interaction landscape in which
604 associations between host health and microbiome abundance can be extremely taxon-
605 specific, displaying functional heterogeneity at the species level. Building a baseline
606 understanding of the resolution at which genetic associations change for different
607 lineages is vital to build an understanding of health, function, and coevolution in
608 microbe-host models.

609 We perform parallel analyses to find specific associations between genetic loci and
610 individual taxonomic groups, treating sub-clades as independent phenotypes from their
611 parent taxa during QTL calculations. This setup allows us to contextualize significant
612 QTL across the bacterial taxonomy, and we find similarities in both the genomic regions
613 detected and the functional annotation of covered genes for taxa in the same clade. We
614 also greatly benefit from the type of QTL analysis facilitated by the DO mouse model,
615 where the genotype for specific loci can be calculated and contrasted consistently
616 across all samples, eliminating the need for the windowed confidence intervals which
617 are common in this type of analysis.

618 We find functional associations in the gene sets identified by the QTL results that
619 span disease and development phenotypes beyond obesity. We find QTL regions
620 spanning genes with annotations for various phenotypes that are already widely studied
621 in the context of host-microbiome interactions. Among them we see cancer-associated
622 annotations, both in the more obvious gastrointestinal categories like colorectal cancer
623 (CHEN *et al.* 2012; AHN *et al.* 2013, ZACKULAR *et al.* 2014; ERICSSON *et al.* 2015) and the
624 surprising, but well-studied, breast (YANG *et al.* 2017; FERNÁNDEZ *et al.* 2018; ZHU *et al.*
625 2018), ovarian (XU *et al.* 2020), and liver cancers (YU AND SCHWABE 2017). We also see
626 an expected plethora of immune and inflammatory pathways, including some
627 microbiome-associated disease hallmarks, including colitis (KNOX *et al.* 2019), allergic
628 response (Pascal *et al.* 2018), and atopic dermatitis (KIM AND KIM 2019). Beyond
629 pathology, we see an enrichment of lipid metabolism pathways, coherent with the gut
630 microbiome's direct and indirect role in host lipid modulation (GHAZALPOUR *et al.* 2016;
631 HEAVER *et al.* 2018; BROWN *et al.* 2019; JOHNSON *et al.* 2019).

632 The relationship between a host's health and their microbiome seems increasingly
633 complex. Links to host development, disease, and metabolism are still being found
634 across body sites and a wealth of bioinformatic and modelling strategies continue to
635 emerge (MALLA *et al.* 2019). These results are a promising and heavily funded target for
636 precision medicine (PROCTOR *et al.* 2019), identifying potential biomarkers for
637 predisposition to type 1 diabetes (UUSITALO *et al.* 2016) and asthma (DURACK *et al.*
638 2018) in children, and colorectal cancer in adults (SHAH *et al.* 2018). As we move
639 forward to understand the mechanisms underlying host-health modulation by the
640 microbiome, it is imperative that we understand which parts of host genomes might

641 have underlying associations with microbial species, both to understand the limitations
642 of animal models as a relevant human proxy, and to determine whether host genetics
643 plays a causal role.

644 Currently, there is a scarcity of studies discussing heritabilities and QTL mappings
645 of bacteria within the gut microbiome. Despite the potential and funding of this field,
646 there is still an absence of a standardized methodology for performing these studies
647 that leads to the use of different procedures and analytical methods, making it
648 increasingly difficult to compare results across studies (GOODRICH *et al.* 2017;
649 KURILSHIKOV *et al.* 2020). We see this in our comparisons of results with previous
650 studies, as we do not observe consistent overlap in the estimated heritabilities and QTL
651 associations in any one taxa. Depending on the study, we see differences in which
652 covariates are able to be included, which databases or mapping algorithms are used to
653 determine OTUs, and the manner in which results are reported. One salient example is
654 our use of both the kinship matrix and co-housing as a random effect in our analysis,
655 which required a tailored approach that extended the standard DO mice pipeline, which
656 usually only allows a kinship matrix as random effect. Ultimately, the current state of the
657 field for profiling different characteristics of the gut microbiome is still rapidly evolving
658 and as it matures and more studies are undertaken, it will become easier to compare,
659 validate, and aggregate results.

660 Although our results support the claim that host genetics can impact the gut
661 microbiome composition in ways that are relevant to the health of the host, our study
662 has some limitations. There is significant room for improvement in the statistical power
663 of this study design through an increase in sample size (currently n = 247 DO mice).

664 Conducting QTL mapping with small sample sizes may lead to the 'Beavis effect' which
665 is a failure to detect QTL of small effect sizes as well as an overestimation of effect size
666 of the QTL that are discovered (MILES AND WAYNE 2008). Our study is also subject to the
667 trade-offs inherent in the Diversity Outbred design: since the genome of each mouse is
668 a unique mixture of the 8 strains from the CC population, the genotype of each DO
669 mouse is independent from other DO mice, and is irreproducible. This hampers the
670 ability to generate biological replicates relative to inbred models, which in turn makes
671 replicating results from the DO population limited to replication of marginal genetic
672 effects. However, this limitation can be partially circumvented by using the CC lines as a
673 form of validation, since they can provide reproducible genotypes (SVENSON *et al.* 2012).
674 Finally, associations between host genetics, microbiome abundance, and functional
675 pathways must be investigated experimentally to confirm mechanism and causality.
676 This is particularly difficult in the overlap of microbiome and genetic association, as
677 hypothesis generation is a challenging and often gene-specific approach which must
678 account for variation in both host and microbial communities.

679 Our results provide insight into the complex interplay between host genetics and
680 the gut microbiome, and isolate associations between microbial taxa and QTL. Overall,
681 this is a challenging analytical setup as we are trying to associate locus-specific
682 variation with several inter-dependent phenotypes in a system with several covariates.
683 Microbiome analyses are very sensitive to the traits, population, and environment under
684 study, which we mitigate by taking into account co-housing and relatedness while also
685 performing computationally intensive permutation tests to provide empirical *p*-values on
686 our most significant QTL hits. As it stands, this method could be further utilized in a

687 study with a novel microbial colonization (or other microbiome perturbation), where
688 measuring the same phenotypes, in a similar setup, could be used to estimate the
689 heritability and identify QTL for the successful introduction of a new taxon (or response
690 to some other perturbation).

691 While most of the variation in the gut microbiome composition is not due to
692 genetics but rather environmental factors (ROTHSCHILD *et al.* 2018), attributes of the gut
693 microbiome that are clearly heritable may provide important insights about host-
694 microbiome interactions and the mechanisms that impact microbiome composition. As
695 the microbiome field moves toward novel disease models, biomarkers, and treatments,
696 it is imperative that we understand the host-genetic variation that might influence the
697 appropriateness of our models, the accuracy of our biomarkers, and the efficacy of new
698 treatments.

ACKNOWLEDGMENTS

The authors want to thank Noah Clark, Jessica L. Sutter, Qiaojuan Shi, Emily Davenport, and Afrah Shafquat for all the help and advice provided. F.S. was supported by a Presidential Life Science Fellowship (PLSF) from Cornell University. This work was supported by NIH grant R01 GM 070683.

AUTHOR CONTRIBUTIONS

F.S., A.G.C, G.A.C, and R.E.L. conceived the study. A.P. provided the samples. F.S. extracted and generated the 16S rRNA gene sequencing data. F.S., E.J.C., P.S., J.K.G., R.E.L., G.A.C, and A.G.C. conceived the computational and statistical analyses. F.S., D.Y.Z., E.J.C., J.F.B., M.E., and P.S. performed the computational and statistical analyses. F.S., J.F.B., D.Y.Z., E.J.C, and A.G.C. wrote the manuscript.

SUPPLEMENTAL MATERIAL

File S1 - Analysis on rarefied data. Detailed breakdown of variation of gut microbiota, heritability estimates, and QTL association results for rarefied data.

Figure S1 - **Taxa relative abundance frequencies.** Stacked bar plots and box plots depicting relative abundance frequencies of the top ten most abundant taxa for each of five taxonomic levels. Relative abundance frequencies are plotted for taxa levels from both the non-rarefied and the rarefied datasets.

Figure S2 - Heatmaps showing the genes involved in any function that were found enriched by IPA gene set analysis. Taxon-specific analysis on genes in the QTL regions associated with relative abundance of phylum Firmicutes **(A)**, genus *Staphylococcus* **(B)**, family Ruminococcaceae **(C)**, class Mollicutes **(D)**, and order Bacteroidales **(E)**. We only show annotations with a False Discovery rate under 3% after multiple-hypothesis correction. Filled-in cells indicate that

722 the gene listed at the top of that column is annotated with the function or disease of that row. Only
723 genes in the gene set of interest are shown, these charts do not display all gene members of each
724 pathway.

725 **Figure S3 - Correlation plot between non-rarefied and rarefied taxa.** Heatmap
726 depicting the Pearson correlations between the relative common taxa relative abundances in non-
727 rarefied (NonR) and rarefied (R) data, revealing that the same taxa from both non-rarefied and
728 rarefied datasets always group closer together than with other taxa, followed by taxa belonging to the
729 same clade.

730 **Figure S4 - Proportion of variance estimates for kinship and cage for all taxa in**
731 **rarefied data.** Proportion of variance estimates for kinship (green), cage effects (orange), and
732 unexplained residual effects (blue) for each taxon. The kinship proportion of variance is an estimate
733 of narrow sense heritability. Heritability percentages are shown on the left. Heritability standard error
734 values are shown with black horizontal lines. Designations p_, c_, o_, f_, and g_ are for phylum,
735 class, order, family, and genus, respectively. When results are identical across taxa in the same
736 phylogenetic branch, only the lowest (most specific) taxa are shown and the rest are shaded out.
737 Heritability significance is marked with one plus (**+**, RLTR *p*-value < 0.05) and BH FDR is shown in
738 parentheses next to heritability percentages. Taxa marked with a red asterisk have statistically
739 suggestive QTL (*, adj. *p*-value < 0.1). Complete table of heritability results, including non-rarefied
740 data, can be found in **Table S3**.

741 **Figure S5 - Comparison of heritability estimates between non-rarefied and**
742 **rarefied taxa**. Circles with purple fill correspond to non-rarefied taxa with statistically significant
743 heritabilities. Circles with green outlines correspond to rarefied taxa with statistically significant
744 heritabilities. Standard errors are shown as horizontal blue lines for non-rarefied taxa and vertical
745 orange lines for rarefied taxa.

746 **Table S1 - Relative abundance of OTUs.** Relative microbial abundance at the OTU level for
747 each DO mouse in non-rarefied data (**A**) and rarefied data (**B**).

748 **Table S2 - Microbial relative abundance summarized at five levels of taxonomy.**

749 Relative microbial abundance summarized at five levels of taxonomy (phylum, class, order, family,
750 and genus) for each DO mouse in non-rarefied data (**A**) and rarefied data (**B**).

751 **Table S3 - Heritability results at five taxonomic levels.** Complete heritability
752 measurements (h^2) as well as their respective *p*-values, adjusted *p*-values, and standard errors for all
753 tested taxonomies at the five taxonomic levels from the non-rarefied (**A**) and rarefied (**B**) datasets.

754 **Table S4 - QTL results at five taxonomic levels.** QTL regions and their respective *p*-values,
755 permutation *p*-values (when applicable), and genes found within the QTL interval at the five
756 taxonomic levels from the non-rarefied (**A**) and rarefied (**B**) datasets.

757 **Table S5 - Genes within QTL regions with suggestive permutation *p*-value.** Detailed
758 annotations for all genes found within QTL regions with a permutation *p*-value <0.1 at the five
759 taxonomic levels.

760 **Table S6 - QTL results at OTU level in non-rarefied dataset.** QTL regions and their
761 respective *p*-values, permutation *p*-values (when applicable), and genes found within the QTL interval
762 at the OTU level from the non-rarefied dataset.

763 **Table S7 - Comparison of heritabilities and QTL with other studies.** Comparison of
764 taxa heritabilities and QTL from our analyses with other studies across mouse, human, and pig
765 studies (**A**). Information on source studies for heritability values in (**B**) and for QTL/GWAS in (**C**). Full
766 human to mouse synteny mapping results for human studies in (**D**).

767 **Table S8 - Gene network relationships from Figure 8.** Annotated relationships between the
768 genes in network 1 (**A**), network 2 (**B**), and network 3 (**C**) from **Figure 8**.

769 **Table S9 - Functional annotation table from IPA analysis.** Detailed functional annotations
770 from cumulative gene set enrichment analysis using IPA on 1423 genes associated with non-rarefied
771 microbiome abundance.

LITERATURE CITED

Ahn, J., R. Sinha, Z. Pei, C. Dominianni, J. Wu *et al.*, 2013 Human gut microbiome and risk for colorectal cancer. Journal of the National Cancer Institute 105**:** 1907-1911.

Battaglioli, E. J., and P. C. Kashyap, 2018 Chapter 33 - Diet Effects on Gut Microbiome Composition, Function, and Host Physiology, pp. 755-766 in *Physiology of the Gastrointestinal Tract (Sixth Edition)*, edited by H. M. Said. Academic Press.

Belheouane, M., Y. Gupta, S. Künzel, S. Ibrahim and J. F. Baines, 2017 Improved detection of gene-microbe interactions in the mouse skin microbiota using high-resolution QTL mapping of 16S rRNA transcripts. Microbiome 5**:** 59.

Benjamini, Y., and Y. Hochberg, 1995 Controlling the False Discovery Rate: A Practical and Powerful Approach to Multiple Testing. Journal of the Royal Statistical Society. Series B (Methodological) 57**:** 289-300.

Benson, A. K., S. A. Kelly, R. Legge, F. Ma, S. J. Low *et al.*, 2010 Individuality in gut microbiota composition is a complex polygenic trait shaped by multiple environmental and host genetic factors. Proceedings of the National Academy of Sciences 107**:** 18933-18938.

Blekhman, R., J. K. Goodrich, K. Huang, Q. Sun, R. Bukowski *et al.*, 2015 Host genetic variation impacts microbiome composition across human body sites. Genome Biology 16**:** 191.

Bonder, M. J., A. Kurilshikov, E. F. Tigchelaar, Z. Mujagic, F. Imhann *et al.*, 2016 The effect of host genetics on the gut microbiome. Nature Genetics 48**:** 1407.

794 Brown, E. M., X. Ke, D. Hitchcock, S. Jeanfavre, J. Avila-Pacheco *et al.*, 2019
795 *Bacteroides*-derived sphingolipids are critical for maintaining intestinal
796 homeostasis and symbiosis. Cell Host & Microbe 25**:** 668-680.e667.

797 Bubier, J., V. Philip, C. Quince, J. Campbell, Y. Zhou *et al.*, 2018 Systems genetic
798 discovery of host-microbiome interactions reveals mechanisms of microbial
799 involvement in disease. bioRxiv.

800 Camarinha-Silva, A., M. Maushammer, R. Wellmann, M. Vital, S. Preuss *et al.*, 2017
801 Host Genome Influence on Gut Microbial Composition and Microbial Prediction of
802 Complex Traits in Pigs. Genetics 206**:** 1637-1644.

803 Caporaso, J. G., J. Kuczynski, J. Stombaugh, K. Bittinger, F. D. Bushman *et al.*, 2010
804 QIIME allows analysis of high-throughput community sequencing data. Nature
805 methods 7**:** 335-336.

806 Caporaso, J. G., C. L. Lauber, W. A. Walters, D. Berg-Lyons, C. A. Lozupone *et al.*,
807 2011 Global patterns of 16S rRNA diversity at a depth of millions of sequences
808 per sample. Proceedings of the National Academy of Sciences of the United
809 States of America 108 Suppl 1**:** 4516-4522.

810 Chen, D., Z. Yang, X. Chen, Y. Huang, B. Yin *et al.*, 2014 The effect of *Lactobacillus*
811 *rhamnosus* hsryfm 1301 on the intestinal microbiota of a hyperlipidemic rat
812 model. BMC complementary and alternative medicine 14**:** 386-386.

813 Chen, W., F. Liu, Z. Ling, X. Tong and C. Xiang, 2012 Human Intestinal Lumen and
814 Mucosa-Associated Microbiota in Patients with Colorectal Cancer. PLOS ONE 7**:**
815 e39743.

816 Churchill, G. A., D. M. Gatti, S. C. Munger and K. L. Svenson, 2012 The Diversity
817 Outbred mouse population. Mammalian genome : official journal of the
818 International Mammalian Genome Society 23**:** 713-718.

819 Collaborative Cross Consortium, 2012 The genome architecture of the Collaborative
820 Cross mouse genetic reference population. Genetics 190**:** 389-401.

821 Dash, N. R., G. Khoder, A. M. Nada and M. T. Al Bataineh, 2019 Exploring the impact of
822 Helicobacter pylori on gut microbiome composition. PLOS ONE 14**:** e0218274.

823 Davenport, E. R., D. A. Cusanovich, K. Michelini, L. B. Barreiro, C. Ober *et al.*, 2015
824 Genome-Wide Association Studies of the Human Gut Microbiota. PLOS ONE 10**:**
825 e0140301.

826 Dudek-Wicher, R. K., A. Junka and M. Bartoszewicz, 2018 The influence of antibiotics
827 and dietary components on gut microbiota. Prz Gastroenterol 13**:** 85-92.

828 Durack, J., N. E. Kimes, D. L. Lin, M. Rauch, M. McKean *et al.*, 2018 Delayed gut
829 microbiota development in high-risk for asthma infants is temporarily modifiable
830 by *Lactobacillus* supplementation. Nature Communications 9**:** 707.

831 Ericsson, A. C., S. Akter, M. M. Hanson, S. B. Busi, T. W. Parker *et al.*, 2015 Differential
832 susceptibility to colorectal cancer due to naturally occurring gut microbiota.
833 Oncotarget 6**:** 33689-33704.

834 Fava, F., J. Lovegrove, R. Gitau, K. Jackson and K. Tuohy, 2006 The gut microbiota
835 and lipid metabolism: implications for human health and coronary heart disease.
836 Current medicinal chemistry 13**:** 3005-3021.

837 Fernández, M. F., I. Reina-Pérez, J. M. Astorga, A. Rodríguez-Carrillo, J. Plaza-Díaz *et*
838 *al.*, 2018 Breast Cancer and Its Relationship with the Microbiota. International
839 journal of environmental research and public health 15**:** 1747.

840 Francino, M. P., 2016 Antibiotics and the Human Gut Microbiome: Dysbioses and
841 Accumulation of Resistances. Frontiers in Microbiology 6.

842 Gao, C., B. P. Ganesh, Z. Shi, R. R. Shah, R. Fultz *et al.*, 2017 Gut Microbe-Mediated
843 Suppression of Inflammation-Associated Colon Carcinogenesis by Luminal
844 Histamine Production. The American Journal of Pathology 187**:** 2323-2336.

845 Garrett, W. S., J. I. Gordon and L. H. Glimcher, 2010 Homeostasis and inflammation in
846 the intestine. Cell 140**:** 859-870.

847 Gatti, D. M., K. L. Svenson, A. Shabalin, L.-Y. Wu, W. Valdar *et al.*, 2014 Quantitative
848 trait locus mapping methods for diversity outbred mice. G3 (Bethesda, Md.) 4**:**
849 1623-1633.

850 Ghazalpour, A., I. Cespedes, B. J. Bennett and H. Allayee, 2016 Expanding role of gut
851 microbiota in lipid metabolism. Current opinion in lipidology 27**:** 141-147.

852 Goodrich, J. K., E. R. Davenport, M. Beaumont, M. A. Jackson, R. Knight *et al.*, 2016
853 Genetic Determinants of the Gut Microbiome in UK Twins. Cell host & microbe
854 19**:** 731-743.

855 Goodrich, J. K., E. R. Davenport, A. G. Clark and R. E. Ley, 2017 The Relationship
856 Between the Human Genome and Microbiome Comes into View. Annual review
857 of genetics 51**:** 413-433.

858 Goodrich, Julia K., Jillian L. Waters, Angela C. Poole, Jessica L. Sutter, O. Koren *et al.*,
859 2014 Human Genetics Shape the Gut Microbiome. Cell 159**:** 789-799.

860 Heaver, S. L., E. L. Johnson and R. E. Ley, 2018 Sphingolipids in host–microbial
861 interactions. Current Opinion in Microbiology 43**:** 92-99.

862 Hughes, D. A., R. Bacigalupe, J. Wang, M. C. Rühlemann, R. Y. Tito *et al.*, 2020
863 Genome-wide associations of human gut microbiome variation and implications
864 for causal inference analyses. Nature Microbiology.

865 Igartua, C., E. R. Davenport, Y. Gilad, D. L. Nicolae, J. Pinto *et al.*, 2017 Host genetic
866 variation in mucosal immunity pathways influences the upper airway microbiome.
867 Microbiome 5**:** 16.

868 Johnson, E. L., S. L. Heaver, J. L. Waters, B. I. Kim, A. Bretin *et al.*, 2019 Sphingolipid
869 production by gut Bacteroidetes regulates glucose homeostasis. bioRxiv**:**
870 632877.

871 Kang, H. M., J. H. Sul, S. K. Service, N. A. Zaitlen, S.-y. Kong *et al.*, 2010 Variance
872 component model to account for sample structure in genome-wide association
873 studies. Nature Genetics 42**:** 348.

874 Kemis, J. H., V. Linke, K. L. Barrett, F. J. Boehm, L. L. Traeger *et al.*, 2019 Genetic
875 determinants of gut microbiota composition and bile acid profiles in mice. PLOS
876 Genetics 15**:** e1008073.

877 Kim, J. E., and H. S. Kim, 2019 Microbiome of the Skin and Gut in Atopic Dermatitis
878 (AD): Understanding the Pathophysiology and Finding Novel Management
879 Strategies. Journal of clinical medicine 8**:** 444.

880 Knox, N. C., J. D. Forbes, G. Van Domselaar and C. N. Bernstein, 2019 The Gut
881 Microbiome as a Target for IBD Treatment: Are We There Yet? Curr Treat
882 Options Gastroenterol 17**:** 115-126.

883 Kurilshikov, A., C. Medina-Gomez, R. Bacigalupe, D. Radjabzadeh, J. Wang *et al.*, 2020
884 Genetics of human gut microbiome composition. bioRxiv**:**
885 2020.2006.2026.173724.

886 Leamy, L. J., S. A. Kelly, J. Nietfeldt, R. M. Legge, F. Ma *et al.*, 2014 Host genetics and
887 diet, but not immunoglobulin A expression, converge to shape compositional
888 features of the gut microbiome in an advanced intercross population of mice.
889 Genome biology 15**:** 552-552.

890 Ley, R. E., F. Bäckhed, P. Turnbaugh, C. A. Lozupone, R. D. Knight *et al.*, 2005 Obesity
891 alters gut microbial ecology. Proceedings of the National Academy of Sciences of
892 the United States of America 102**:** 11070-11075.

893 Lim, M. Y., H. J. You, H. S. Yoon, B. Kwon, J. Y. Lee *et al.*, 2017 The effect of
894 heritability and host genetics on the gut microbiota and metabolic syndrome. Gut
895 66**:** 1031.

896 Malla, M. A., A. Dubey, A. Kumar, S. Yadav, A. Hashem *et al.*, 2019 Exploring the
897 Human Microbiome: The Potential Future Role of Next-Generation Sequencing in
898 Disease Diagnosis and Treatment. Frontiers in Immunology 9.

899 McFarland, L. V., C. T. Evans and E. J. C. Goldstein, 2018 Strain-Specificity and
900 Disease-Specificity of Probiotic Efficacy: A Systematic Review and Meta-
901 Analysis. Frontiers in medicine 5**:** 124-124.

902 McKnite, A. M., M. E. Perez-Munoz, L. Lu, E. G. Williams, S. Brewer *et al.*, 2012 Murine
903 Gut Microbiota Is Defined by Host Genetics and Modulates Variation of Metabolic
904 Traits. PLOS ONE 7**:** e39191.

905 McMurdie, P. J., and S. Holmes, 2014 Waste Not, Want Not: Why Rarefying
906 Microbiome Data Is Inadmissible. PLOS Computational Biology 10**:** e1003531.

907 Miles, C. M., and M. Wayne, 2008 Quantitative trait locus (QTL) analysis. Nature
908 Education 1**:** 208.

909 Müller, M. J., C. Geisler, J. Blundell, A. Dulloo, Y. Schutz *et al.*, 2018 The case of
910 GWAS of obesity: does body weight control play by the rules? International
911 Journal of Obesity 42**:** 1395-1405.

912 O'Connor, A., P. M. Quizon, J. E. Albright, F. T. Lin and B. J. Bennett, 2014
913 Responsiveness of cardiometabolic-related microbiota to diet is influenced by
914 host genetics. Mammalian genome : official journal of the International
915 Mammalian Genome Society 25**:** 583-599.

916 Org, E., B. W. Parks, J. W. J. Joo, B. Emert, W. Schwartzman *et al.*, 2015 Genetic and
917 environmental control of host-gut microbiota interactions. Genome research 25**:**
918 1558-1569.

919 Ottman, N., J. Reunanen, M. Meijerink, T. E. Pietilä, V. Kainulainen *et al.*, 2017 Pili-like
920 proteins of *Akkermansia muciniphila* modulate host immune responses and gut
921 barrier function. PLOS ONE 12**:** e0173004.

922 Pascal, M., M. Perez-Gordo, T. Caballero, M. M. Escribese, M. N. Lopez Longo *et al.*,
923 2018 Microbiome and Allergic Diseases. Frontiers in immunology 9**:** 1584-1584.

924 Proctor, L., J. LoTempio, A. Marquitz, P. Daschner, D. Xi *et al.*, 2019 A review of 10
925 years of human microbiome research activities at the US National Institutes of
926 Health, Fiscal Years 2007-2016. Microbiome 7**:** 31.

927 Ridaura, V. K., J. J. Faith, F. E. Rey, J. Cheng, A. E. Duncan *et al.*, 2013 Gut microbiota
928 from twins discordant for obesity modulate metabolism in mice. Science (New
929 York, N.Y.) 341**:** 1241214-1241214.

930 Rideout, J. R., Y. He, J. A. Navas-Molina, W. A. Walters, L. K. Ursell *et al.*, 2014
931 Subsampled open-reference clustering creates consistent, comprehensive OTU
932 definitions and scales to billions of sequences. PeerJ 2**:** e545-e545.

933 Rothschild, D., O. Weissbrod, E. Barkan, A. Kurilshikov, T. Korem *et al.*, 2018
934 Environment dominates over host genetics in shaping human gut microbiota.
935 Nature 555**:** 210.

936 Round, J. L., and S. K. Mazmanian, 2009 The gut microbiota shapes intestinal immune
937 responses during health and disease. Nature reviews. Immunology 9**:** 313-323.

938 Scheipl, F., S. Greven and H. Küchenhoff, 2008 Size and power of tests for a zero
939 random effect variance or polynomial regression in additive and linear mixed
940 models. Computational Statistics & Data Analysis 52**:** 3283-3299.

941 Shah, M. S., T. Z. DeSantis, T. Weinmaier, P. J. McMurdie, J. L. Cope *et al.*, 2018
942 Leveraging sequence-based faecal microbial community survey data to identify a
943 composite biomarker for colorectal cancer. Gut 67**:** 882.

944 Shin, J., S. Lee, M.-J. Go, S. Y. Lee, S. C. Kim *et al.*, 2016 Analysis of the mouse gut
945 microbiome using full-length 16S rRNA amplicon sequencing. Scientific Reports
946 6**:** 29681.

947 Snijders, A. M., S. A. Langley, Y.-M. Kim, C. J. Brislawn, C. Noecker *et al.*, 2016
948 Influence of early life exposure, host genetics and diet on the mouse gut
949 microbiome and metabolome. Nature Microbiology 2**:** 16221.

950 Speakman, J. R., R. J. F. Loos, S. O'Rahilly, J. N. Hirschhorn and D. B. Allison, 2018
951 GWAS for BMI: a treasure trove of fundamental insights into the genetic basis of
952 obesity. International Journal of Obesity 42**:** 1524-1531.

953 Svenson, K. L., D. M. Gatti, W. Valdar, C. E. Welsh, R. Cheng *et al.*, 2012 High-
954 Resolution Genetic Mapping Using the Mouse Diversity Outbred Population.
955 Genetics 190**:** 437-447.

956 Turnbaugh, P. J., 2017 Microbes and Diet-Induced Obesity: Fast, Cheap, and Out of
957 Control. Cell host & microbe 21**:** 278-281.

958 Turnbaugh, P. J., M. Hamady, T. Yatsunenko, B. L. Cantarel, A. Duncan *et al.*, 2009 A
959 core gut microbiome in obese and lean twins. Nature 457**:** 480-484.

960 Turpin, W., O. Espin-Garcia, W. Xu, M. S. Silverberg, D. Kevans *et al.*, 2016
961 Association of host genome with intestinal microbial composition in a large
962 healthy cohort. Nature Genetics 48**:** 1413-1417.

963 Uusitalo, U., X. Liu, J. Yang, C. A. Aronsson, S. Hummel *et al.*, 2016 Association of
964 Early Exposure of Probiotics and Islet Autoimmunity in the TEDDY Study. JAMA
965 Pediatr 170**:** 20-28.

966 Veiga, P., C. A. Gallini, C. Beal, M. Michaud, M. L. Delaney *et al.*, 2010 Bifidobacterium
967 animalis subsp. lactis fermented milk product reduces inflammation by altering a
968 niche for colitogenic microbes. Proceedings of the National Academy of Sciences
969 of the United States of America 107**:** 18132-18137.

970 Vorobyev, A., Y. Gupta, T. Sezin, H. Koga, Y. C. Bartsch *et al.*, 2019 Gene-diet
971 interactions associated with complex trait variation in an advanced intercross
972 outbred mouse line. Nature Communications 10**:** 4097.

973 Wang, J., S. Kalyan, N. Steck, L. M. Turner, B. Harr *et al.*, 2015 Analysis of intestinal
974 microbiota in hybrid house mice reveals evolutionary divergence in a vertebrate
975 hologenome. Nature Communications 6**:** 6440.

976 Wang, J., L. B. Thingholm, J. Skiecevičienė, P. Rausch, M. Kummen *et al.*, 2016
977 Genome-wide association analysis identifies variation in vitamin D receptor and
978 other host factors influencing the gut microbiota. Nature genetics 48**:** 1396-1406.

979 Weiss, S., Z. Z. Xu, S. Peddada, A. Amir, K. Bittinger *et al.*, 2017 Normalization and
980 microbial differential abundance strategies depend upon data characteristics.
981 Microbiome 5**:** 27.

982 Wen, L., R. E. Ley, P. Y. Volchkov, P. B. Stranges, L. Avanesyan *et al.*, 2008 Innate
983 immunity and intestinal microbiota in the development of Type 1 diabetes. Nature
984 455**:** 1109-1113.

985 Xu, J., J.-J. Peng, W. Yang, K. Fu and Y. Zhang, 2020 Vaginal microbiomes and
986 ovarian cancer: a review. American journal of cancer research 10**:** 743-756.

987 Yang, J., Q. Tan, Q. Fu, Y. Zhou, Y. Hu *et al.*, 2017 Gastrointestinal microbiome and
988 breast cancer: correlations, mechanisms and potential clinical implications.
989 Breast Cancer 24**:** 220-228.

990 Yu, L.-X., and R. F. Schwabe, 2017 The gut microbiome and liver cancer: mechanisms
991 and clinical translation. Nature Reviews Gastroenterology & Hepatology 14**:** 527-
992 539.

993 Zackular, J. P., M. A. M. Rogers, M. T. Ruffin and P. D. Schloss, 2014 The Human Gut
994 Microbiome as a Screening Tool for Colorectal Cancer. Cancer Prevention
995 Research 7**:** 1112.

996 Zhai, R., X. Xue, L. Zhang, X. Yang, L. Zhao *et al.*, 2019 Strain-Specific Anti-
997 inflammatory Properties of Two Akkermansia muciniphila Strains on Chronic
998 Colitis in Mice. Frontiers in Cellular and Infection Microbiology 9.

999 Zhu, J., M. Liao, Z. Yao, W. Liang, Q. Li *et al.*, 2018 Breast cancer in postmenopausal
1000 women is associated with an altered gut metagenome. Microbiome 6**:** 136.

1001 Ziyatdinov, A., M. Vázquez-Santiago, H. Brunel, A. Martinez-Perez, H. Aschard *et al.*,
1002 2018 lme4qtl: linear mixed models with flexible covariance structure for genetic
1003 studies of related individuals. BMC bioinformatics 19**:** 68-68.